JCI The Journal of Clinical Investigation

Lysophospholipid acylation modulates plasma membrane lipid organization and insulin sensitivity in skeletal muscle

Patrick J. Ferrara, … , William L. Holland, Katsuhiko Funai

J Clin Invest. 2021. https://doi.org/10.1172/JCI135963.

Research In-Press Preview **Metabolism** **Muscle biology**

Aberrant lipid metabolism promotes the development of skeletal muscle insulin resistance, but the exact identity of lipid-mediated mechanisms relevant to human obesity remains unclear. A comprehensive lipidomic analysis of primary myocytes from lean insulin-sensitive (LN) and obese insulin-resistant (OB) individuals revealed several species of lysophospholipids (lyso-PL) that were differentially-abundant. These changes coincided with greater expression of lysophosphatidylcholine acyltransferase 3 (LPCAT3), an enzyme involved in phospholipid transacylation (Lands cycle). Strikingly, mice with skeletal muscle-specific knockout of LPCAT3 (LPCAT3-MKO) exhibited greater muscle lyso-PC/PC, concomitant with improved skeletal muscle insulin sensitivity. Conversely, skeletal muscle-specific overexpression of LPCAT3 (LPCAT3-MKI) promoted glucose intolerance. The absence of LPCAT3 reduced phospholipid packing of cellular membranes and increased plasma membrane lipid clustering, suggesting that LPCAT3 affects insulin receptor phosphorylation by modulating plasma membrane lipid organization. In conclusion, obesity accelerates the skeletal muscle Lands cycle, whose consequence might induce the disruption of plasma membrane organization that suppresses muscle insulin action.

Lysophospholipid acylation modulates plasma membrane lipid organization and insulin sensitivity in skeletal muscle

Patrick J. Ferrara,[1-5] Xin Rong,[6] J. Alan Maschek,[1,7] Anthony R.P. Verkerke,[1-4] Piyarat Siripoksup,[1,8] Haowei Song,[9] Thomas D. Green,[3] Karthickeyan C. Krishnan,[10] Jordan M. Johnson,[1-4] John Turk,[9] Joseph A. Houmard,[3,4] Aldons J. Lusis,[10] Micah J. Drummond,[1,5,8] Joseph M. McClung,[3] James E. Cox,[1,7,11] Saame Raza Shaikh,[3,12] Peter Tontonoz,[6] William L. Holland,[1,2,5] *Katsuhiko Funai[1-5,8]*

[1]Diabetes and Metabolism Research Center, University of Utah, Salt Lake City, UT, USA

[2]Department of Nutrition and Integrative Physiology, University of Utah, Salt Lake City, UT, USA

[3]East Carolina Diabetes and Obesity Institute, East Carolina University, Greenville, NC, USA

[4]Human Performance Laboratory, East Carolina University, Greenville, NC, USA

[5]Molecular Medicine Program, University of Utah, Salt Lake City, UT, USA

[6]Department of Pathology and Laboratory Medicine, University of California, Los Angeles, Los Angeles, CA, USA

[7]Metabolomics, Mass Spectrometry, and Proteomics Core, University of Utah, Salt Lake City, UT, USA

[8]Department of Physical Therapy and Athletic Training, University of Utah, Salt Lake City, UT, USA

[9]Division of Endocrinology Metabolism and Lipid Research, School of Medicine, Washington University in St. Louis, St. Louis, MO, USA

[10]Department of Medicine, Cardiology Division at the University of California Los Angeles, Los Angeles, CA, USA

[11]Department of Biochemistry, University of Utah, Salt Lake City, UT, USA

[12]Department of Nutrition, University of North Carolina at Chapel Hill, Chapel Hill, NC, USA

*Correspondence:
Katsuhiko Funai, PhD
Diabetes & Metabolism Research Center
15 N, 2030 E, Salt Lake City, UT 84112
Phone: (801) 585-1781
Fax: (801) 585-0701
Email: kfunai@utah.edu

Conflict of Interest

The authors have declared that no conflict of interest exists.

Abstract

Aberrant lipid metabolism promotes the development of skeletal muscle insulin resistance, but the exact identity of lipid-mediated mechanisms relevant to human obesity remains unclear. A comprehensive lipidomic analysis of primary myocytes from individuals that are insulin-sensitive and lean (LN) or insulin-resistant with obesity (OB) revealed several species of lysophospholipids (lyso-PL) that were differentially-abundant. These changes coincided with greater expression of lysophosphatidylcholine acyltransferase 3 (LPCAT3), an enzyme involved in phospholipid transacylation (Lands cycle). Strikingly, mice with skeletal muscle-specific knockout of LPCAT3 (LPCAT3-MKO) exhibited greater muscle lyso-PC/PC, concomitant with improved skeletal muscle insulin sensitivity. Conversely, skeletal muscle-specific overexpression of LPCAT3 (LPCAT3-MKI) promoted glucose intolerance. The absence of LPCAT3 reduced phospholipid packing of cellular membranes and increased plasma membrane lipid clustering, suggesting that LPCAT3 affects insulin receptor phosphorylation by modulating plasma membrane lipid organization. In conclusion, obesity accelerates the skeletal muscle Lands cycle, whose consequence might induce the disruption of plasma membrane organization that suppresses muscle insulin action.

Introduction

Type 2 diabetes is the 7th leading cause of death in the United States (1) and is a major risk factor for cardiovascular disease, the leading cause of death (2). Skeletal muscle is the site of the largest glucose disposal in humans (3, 4). Insulin resistance in skeletal muscle is a necessary precursor to type 2 diabetes (5) and can be triggered by aberrant lipid metabolism (6-8). Several classes of lipids have been implicated in initiating cellular signals that suppress insulin action, but there has not been a clear consensus that these molecules are upregulated in skeletal muscle insulin resistance that occurs in the human population (9-14).

A difficulty in accurately measuring the muscle lipidome is confounded by the intramyofibrillar adipocytes which are particularly abundant in muscle biopsy samples from individuals with obesity. Human skeletal muscle cells (HSkMC) are primary myoblasts that can be isolated, propagated, and differentiated from muscle biopsies. This in vitro system provides a unique model to study the skeletal muscle lipidome and signaling pathways free of contaminating cell types and circulating factors that affect muscle metabolism. Importantly, these HSkMC are known to retain their insulin sensitivity phenotype *ex vivo*, providing a platform to study mechanisms directly relevant to human physiology (15, 16).

In this study, we harvested HSkMC from subjects that are insulin-sensitive and lean (LN) or insulin-resistant with obesity (OB) (Subject Characteristics: Table S1). We then propagated and differentiated these samples for analyses of the muscle lipidome, gene expression profile, insulin signaling, and membrane properties (Figure 1A). This approach led us to examine the lysophospholipid (lyso-PL) remodeling pathway (Lands cycle) as a potential diet-responsive mechanism that regulates skeletal muscle insulin action. Below we provide evidence that implicates this pathway in the pathogenesis of diet-induced skeletal muscle insulin resistance.

Genetic or pharmacologic suppression of this pathway was sufficient to enhance skeletal muscle insulin action in vitro and in vivo.

Results

Human primary muscle cells from OB subjects were more insulin resistant compared to LN controls (15). A global lipidomic analysis of these LN and OB myotubes revealed many classes of lipids that were differentially abundant (Figure 1B, Figure S1A-L). Among these, several species of lysophospholipids (lyso-PL), intermediates of the Lands cycle (17), were lower in OB HSkMC compared to LN (Figure 1C), a finding not previously described for an insulin-resistant state. While species of many classes of lyso-PL were reduced with obesity, the ratio of lyso-PL to its parent phospholipid was significantly lower for only lysophosphatidylcholine (lyso-PC)/phosphatidylcholine (PC) (Figure 1D). Previous studies suggest that altering the lyso-PC content of cell membranes is sufficient to alter the physical properties of membranes (18, 19). Consistent with this notion, phospholipid packing of LN and OB myotubes were remarkably different, with OB cells exhibiting more tightly packed membrane head groups compared to LN (Figure 1E&F). This occurred in the absence of changes in the phospholipid acyl-chain saturation index (Figure S1M).

What is the molecular mechanism by which obesity promotes a lower abundance of lyso-PL in skeletal muscle? LN and OB HSkMC utilized for the lipidomic analyses were cultured *ex vivo* for several weeks in identical media conditions. Thus, differences in the lipidome of these samples are likely the result of genetic and/or epigenetic influences, instead of hormonal or neuronal inputs that alter cells in vivo. We reasoned that such differential programming might be expected to manifest in gene expression profiles. A whole transcriptome sequencing of LN and OB myotubes revealed that lyso-PC acyltransferase 3 (LPCAT3), an enzyme of the Lands cycle, was more highly expressed with obesity (GEO Series accession number: GSE162265).

These findings were recapitulated in muscle biopsy samples (*not* myotubes) from LN and OB individuals as well as muscle tissue from wildtype fed high-fat diet (HFD) or in db/db mice (Figure 1G). The Lands cycle represents a series of phospholipid-remodeling reactions by which acyl-chains become transacylated (17). Of the thirteen lyso-PL acyltransferase enzymes (20), LPCAT3 has the highest affinity for 16:0 and 18:0 lyso-PC, consistent with the specificity of reduced lyso-PC/PC (21, 22). Silencing of LPCAT3 in fibroblasts has been shown to increase Akt phosphorylation (23), while incubation of the same cells with 16:0/20:4 PC decreased Akt phosphorylation due to plasma-membrane specific effects (24). Mice with a liver-specific deletion of LPCAT3 exhibit enhanced ordering of membranes (25). In both human and mouse skeletal muscle, LPCAT3 is very highly expressed compared to other isoforms of LPCAT (Figure 1H), and skeletal muscle LPCAT3 expression is directly correlated to circulating insulin in 106 mouse strains (data not shown, bicor=0.296, P=0.0016) (26).

To study the role of LPCAT3 on skeletal muscle insulin action, we performed a lentivirus-mediated shRNA knockdown of LPCAT3 (Scrambled, SC; LPCAT3 knockdown, KD) in C2C12 myotubes (Figure 2A). LPCAT3 knockdown did not affect protein content for MyoD, various MHC isoforms, and respiratory complexes (Figure S2A-C), suggesting that the deletion of LPCAT3 has no effect on myotube lineage or mitochondrial density. Targeted lipidomic analyses revealed that LPCAT3 knockdown increased lyso-PC and decreased PC (Figure 2B&C), substrates and products of the LPCAT3-mediated reaction, respectively (27, 28). Together, these differences were sufficient to elevate lyso-PC/PC with LPCAT3 deletion (Figure 2D). Similar effects were seen with lipid species composed of an ethanolamine head group (Figure S2D-F), while the phospholipid saturation index increased with LPCAT3 knockdown (Figure S2G). Analogous to differences observed in LN and OB HSkMC, LPCAT3 deletion reduced phospholipid head group packing (Figure 2E&F). We then incubated SC and KD cells in a submaximal concentration of insulin to assess insulin signaling events. Strikingly, inhibition

of LPCAT3 robustly enhanced insulin signaling with or without insulin (Figure 3A, Figure S2H). Notably, the increase occurred at the level of the insulin receptor (IR), a node that is localized in the phospholipid-rich plasma membrane. Consequently, LPCAT3 deletion enhanced insulin-stimulated glycogen synthesis (Figure 3B), suggesting that this intervention increases skeletal muscle insulin sensitivity in vitro (due to low GLUT4:GLUT1 stoichiometry, insulin-stimulated glucose uptake is not an ideal surrogate for insulin sensitivity in C2C12 myotubes). LPCAT3 knockdown also enhanced insulin signaling in HSkMC from subjects with obesity (Figure 3A).

The organization and clustering of plasma membrane microdomains is linked to the induction of tyrosine-kinase signaling events, such as IR signaling (29-31). Because LPCAT3 deletion promoted enhanced insulin signaling at the level of IR phosphorylation, we visualized the organization of plasma membrane microdomains with labeling and patching of plasma membrane GM-1, a known marker of microdomains. Indeed, a greater proportion of C2C12 cells with LPCAT3 knockdown exhibited clustering of GM-1 enriched microdomains (Figure 3C, top &D). Furthermore, LPCAT3 deletion decreased the size of these clusters (Figure 3C, bottom &E), with no differences in total fluorescence from each cell (Figure S2I). These data indicate that LPCAT3 inhibition induces a reorganization of plasma membrane microdomains, potentially explaining increased IR phosphorylation.

CI-976 is a pan lysophospholipid acyltransferase inhibitor (32, 33) that has the ability to disrupt Lands cycle, similar to LPCAT3 deletion. To examine a possibility that the insulin-sensitizing effect of LPCAT3 knockdown is attributable to an unknown function of LPCAT3 outside of the Lands cycle, we studied C2C12 myotubes with or without CI-976. Consistent with our findings with LPCAT3 knockdown (Figure 2E&F), pre-incubation of wildtype C2C12 myotubes with CI-976 robustly decreased phospholipid headgroup packing (Figure 4A&B) and increased insulin-stimulated Akt phosphorylation (Figure 4C&D). We also administered CI-976 to wildtype

(C57BL/6J) mice that have been fed HFD. Strikingly, mice injected with CI-976 exhibited increased glucose tolerance compared to vehicle-treated controls without altering body weights (Figure 4E-G). These evidence support our findings that inhibition of Lands cycle may increase skeletal muscle insulin sensitivity.

As effects of CI-976 administration in vivo cannot be attributed to effects on skeletal muscle alone, we performed skeletal muscle-specific deletion of LPCAT3 in vivo. Mice with tamoxifen-inducible skeletal muscle-specific knock-out of LPCAT3 (LPCAT3-MKO) were generated by crossing the HSA-MerCreMer mice (34) with LPCAT3 conditional knock-out mice (exon3 of the *Lpcat3* gene flanked with *loxP* sites) (25) (Figure 5A). This strategy successfully yielded mice with suppressed LPCAT3 expression in skeletal muscle without affecting other tissues (Figure 5B), and without compensatory upregulation of other members of the LPCAT family (Figure 5C, Figure S3A). Control and LPCAT3-MKO mice gained weight equally when fed a high-fat diet (HFD, Figure 5D) with no difference in adipose tissue weight at the end of diet intervention (Figure 5E). Food consumption, whole-body oxygen consumption, spontaneous activity, and respiratory exchange ratio were similarly not different between groups (Figure 5F-I). Fasting glucose and insulin, and glucose tolerance (Figure 5J&K, 6A) were unchanged, but circulating insulin during the glucose tolerance test was substantially lower in LPCAT3-MKO mice compared to the control group (Figure 6B).

To evaluate whether improved glycemic efficiency was attributable to greater skeletal muscle insulin sensitivity, we subjected HFD-fed control and LPCAT3-MKO mice to hyperinsulinemic-euglycemic clamping experiments. Similar to results from the glucose tolerance test, control and LPCAT3-MKO mice had similar glucose infusion rates (Figure 6C), suggesting comparable systemic insulin sensitivity. Likewise, hepatic glucose output was not different between the groups (Figure 6D). In contrast, glucose disposal rate was approximately 2-fold higher in

LPCAT3-MKO mice compared to control, indicating increased peripheral insulin sensitivity (Figure 6E). Furthermore, infusion of ^{14}C-2-deoxyglucose during the insulin-stimulated clamp phased elevated uptake in soleus and diaphragm muscles from LPCAT3-MKO mice compared to control (Figure 6F). We further validated elevated muscle insulin sensitivity by performing the ^{3}H-2-deoxyglucose uptake assay ex vivo. Indeed, insulin-stimulated skeletal muscle glucose uptake was robustly enhanced in LPCAT3-MKO mice compared to control (Figure 6G). The increase in glucose uptake coincided with augmented insulin-stimulated Akt phosphorylation (Figure 6H&I), similar to C2C12 and human primary myotubes (Figure 3). These results suggest that inhibition of muscle LPCAT3 increases skeletal muscle insulin sensitivity in vivo.

Similar to results from LPCAT3 knockdown in vitro, muscles from LPCAT3-MKO mice had elevated lyso-PC (16:0 and 18:0) (Figure 7A) and lower levels of PC species known to be the main products of the LPCAT3 reaction (16:0/18:2 and 16:0/22:4) (Figure 7B) (22, 35, 36). As a result, lyso-PC/PC was ~2-fold greater in LPCAT3-MKO mice compared to control (Figure 7C). In contrast, lyso-PE/PE or phospholipid saturation index was unaltered between control and LPCAT3-MKO muscles (Figure S3B-E), similar to the lipidome in LN and OB HSkMC (Figure 1&S1). Muscles from control and LPCAT3-MKO did not differ in mass, length, force-generating capacity, fiber-type distribution, or content of proteins in the electron transport chain (Figure 7D-I, Figure S3F-H).

We also explored whether acceleration of the Lands cycle would be sufficient to impair glucose handling. For these experiments, we generated mice with skeletal muscle-specific LPCAT3 overexpression (LPCAT3-MKI). A mouse LPCAT3 cDNA sequence was inserted into the Rosa26 locus preceded by a stop codon, which was flanked with loxP sites to generate LPCAT3 conditional knock-in (LPCAT3cKI+/-) mice (Figure 8A). LPCAT3cKI+/+ mice were crossed with the HSA-MerCreMer+/- mice to generate the control (LPCAT3cKI+/-; HSA-MerCreMer-/-) or

LPCAT3-MKI (LPCAT3cKI+/-; HSA-MerCreMer+/-) mice (Figure 8B). This strategy successfully resulted in LPCAT3 overexpression specific to skeletal muscle (Figure 8C), which was sufficient to accelerate the Lands cycle to reduce lyso-PC (Figure 8D), increase some species of PC (Figure 8E), and reduce lyso-PC/PC ratio (Figure 8F). LPCAT3-MKI mice had similar body weights to littermate controls when fed standard chow or HFD (Figure 8G). Importantly, LPCAT3-MKI mice were found to be more glucose intolerant compared to controls (Figure 8H&I). Thus, acceleration of skeletal muscle Lands cycle is sufficient to impair systemic glucose handling.

How does the inhibition of the Lands cycle promote greater insulin action in skeletal muscle? LPCAT3 deficiency enhanced insulin signaling at the level of IR which was concomitant with altered plasma membrane lipid organization (Figure 3), suggesting that changes in plasma membrane properties may mediate the insulin-sensitizing effects. Membrane organization is vital to insulin action, as IR is localized to highly ordered microdomains on the plasma membrane (37, 38). The interaction between caveolae and IR enhances insulin signaling in other cell types (39, 40). Mice that lack caveolin-3 (cav3), a skeletal muscle-specific scaffolding protein critical in the formation of caveolae on the plasma membrane, exhibit skeletal muscle insulin resistance due to plasma membrane-specific effects on the IR (41, 42). Overexpression of dominant-negative cav3 leads to decreased glucose uptake and glycogen synthesis in C2C12 cells, which is attributed to decreased Akt phosphorylation (43-45). Conversely, an increase in wildtype cav3 expression is sufficient to enhance Akt phosphorylation and glucose uptake (46). Indeed, LPCAT3 knockdown substantially increased cav3 content in C2C12 myotubes (Figure 9A). To examine the possibility that the absence of LPCAT3 increases the abundance of lipids in caveolae, we isolated membrane fractions from C2C12 myotubes with or without LPCAT3 deletion and subjected them for further purification by density-gradient ultracentrifugation.

Cholesterol and sphingomyelin are two classes of lipids that are more highly abundant in the detergent-resistant membrane (DRM; i.e. ordered membrane) fraction compared to the detergent-soluble membrane (DSM) fraction (47). Experiments in wildtype C2C12 myotubes indicated that fractions 4-5 have substantial amounts of total lipid (Figure S5A). These fractions were enriched in sphingomyelin and cholesterol which are known to be conducive for more highly ordered membranes (Figure S5B&C), with a relatively low abundance of lipids involved in the LPCAT3-mediated reaction (Figure S5D-G). LPCAT3 knockdown did not appear to alter the overall content of lipid in the DRM fraction, nor did it affect enrichment of sphingomyelin and cholesterol (Figure 9B&C). Even though the DRM fraction is known to contain very little protein (48), we detected substantial cav3 in both SC and KD myotubes (Figure 9D). While LPCAT3 deletion did not affect the proportion of cav3 in the DRM fraction, it is noteworthy that elevated cav3 content with LPCAT3 knockdown (Figure 9A) is reflected in the DRM fraction. This is particularly interesting considering there was no enrichment of sphingomyelin or cholesterol in the DRM fraction, which may have been expected given that these lipids induce sequestration of cav3 into caveolae. Consistent with this notion, LPCAT3 deletion was sufficient to elevate lyso-PC in the DRM as well as DRM fractions of the membrane (Figure 9E), with minimal effect on PC species (Figure S5A). Similar results were exhibited with lyso-PE and PE (Figure S5B&C). The saturation index of phospholipids was slightly increased in both DRM and DSM fractions, which may also contribute to the increase in the plasma membrane lipid clustering (Figure S5D). Thus, LPCAT3 deletion promotes the accumulation of lyso-PC in the DRM fraction which may contribute to membrane organization. To test our hypothesis that an increase in membrane organization mediates the insulin-sensitizing effect of LPCAT3 deletion, we incubated C2C12 myotubes with methyl-beta-cyclodextrin (MβCD), a cholesterol-depleting compound that disrupts plasma membrane microdomains (49). Indeed, incubation of cells with MβCD decreased cav3 protein content (Figure 10A) without decreasing the abundance of

flotillin-1 (Figure 10B), a protein associated with non-caveolar microdomains. MβCD treatment normalized insulin-stimulated Akt phosphorylation with LPCAT3 deletion to control levels (Figure 10C&D). Finally, we also examined whether alteration of plasma membrane microdomains induced by LPCAT3 deletion would affect other cell-surface receptor-mediated signaling events. For these experiments, we incubated C2C12 myotubes with epidermal growth factor (EGF) or platelet-derived growth factor (PDGF) in addition to insulin with or without LPCAT3 knockdown. Both EGF and PDGF receptors are localized at the plasma membrane and activates Akt independent of IR (50, 51). Strikingly, LPCAT3 deletion did not augment Akt phosphorylation induced by EGF or PDGF (Figure 10E&F), suggesting that the effects of LPCAT3 deletion are selective. These findings are consistent with the notion that LPCAT3 deletion enhances insulin signaling by its effect on plasma membrane organization that is relatively specific to IR.

Discussion

Obesity promotes aberrant lipid metabolism in various tissues including skeletal muscle where it dampens its ability to respond to circulating insulin and increase glucose uptake. Studies in model organisms have led to the identification of lipotoxic lipids that might promote insulin resistance in various tissues (52, 53), but some studies were unable to validate these mechanisms in human muscles (54, 55). To gain a global understanding of changes that occur in muscle lipid metabolism with human obesity, we conducted lipidomic analyses on muscle samples from LN and OB subjects. Obesity was associated with decreases in various species of lysophospholipids, an observation that had never been previously reported. Many of these lipids are generated by the enzymes of the Lands cycle, which removes fatty-acyl chains at the sn-2 position of phospholipids to generate lysophospholipids (Lands cycle). We propose a novel mechanism by which obesity accelerates the skeletal muscle Lands cycle to promote insulin resistance.

The acceleration of muscle phospholipid transacylation was apparently driven by increased LPCAT3 expression, likely attributable to diet-induced activation of LXRs and PPARs (22, 56, 57). Indeed, we found that skeletal muscle-specific overexpression of LPCAT3 was sufficient to augment glucose intolerance induced by HFD feeding. In contrast, inhibition of LPCAT3 enhances insulin signaling at the level of IR to improve skeletal muscle insulin sensitivity. We believe that the insulin-sensitizing effect of Lands cycle inhibition is mediated by its effect on the plasma membrane lipid organization (Figure 11). Consistent with this notion, LPCAT3 deletion and/or CI-976 treatment was sufficient to alter membrane phospholipid packing and GM1-microdomain clustering, cav3 content, and lipid composition of detergent-resistant and –soluble membranes. Furthermore, disruption of cholesterol-rich microdomains was sufficient to eliminate the insulin-sensitizing effect of LPCAT3 inhibition. Interventions that interfere with the plasma membrane organization would be predicted to have effects on other cellular events, but the deletion of LPCAT3 did not alter EGF or PDGF sensitivity, suggesting some specificity for IR. LPCAT3 deletion did not appear to have an overly adverse effect on skeletal muscle, including mass, fiber-type or force-generating capacity. It would be of substantial interest to pursue implications of altered Lands cycle and/or plasma membrane organization in the context of other cellular events. In particular, a recent study suggests that plasma membrane *sn*-1,2-diacylglycerol accumulation promotes PKCε activation, increased IR-Thr1160 phosphorylation, and decreased IR-Tyr1162 phosphorylation in liver (58). Thus, it would be of great interest to examine how changes in Lands cycle alter IR phosphorylation by interacting with this mechanism in muscle.

Observations in this study open up a potential opportunity to pharmacologically target this pathway to enhance skeletal muscle insulin sensitivity. It is noteworthy that the current study partly drew its conclusions from lipidomic analyses and loss-of-function studies performed in

315 human samples, suggesting that this mechanism may be directly involved in the pathogenesis
316 of skeletal muscle insulin resistance in human obesity. We are also interested in examining
317 whether obesity induces similar changes in plasma membrane organization of other tissues to
318 promote pathology.
319

Methods

Human Subjects

All participants were prescreened and/or self-reported to be free of any known metabolic diseases or heart conditions, nontobacco users, not taking any medications known to alter metabolism, and sedentary. Six lean subjects without diabetes (LN: BMI < 25 kg/m^2) and six subjects with severe obesity (OB: BMI > 40 kg/m^2) were studied (all Caucasian females). The subjects were instructed not to exercise for approximately 48h before the muscle biopsy. A fasting blood sample (glucose and insulin) and muscle biopsy from the vastus lateralis were collected. A portion of the biopsy sample was frozen immediately, and another portion was used to isolate primary muscle cells.

Cell Culture

Primary human skeletal muscle cells (HSkMC) were isolated from fresh muscle biopsies as previously described (15, 59). HSkMC were cultured in growth media containing low glucose DMEM, 10x FBS, 0.5 mg/mL BSA, 0.5 mg/mL fetuin, 10 ng/mL human EGF, 1 μM dexamethasone, and 0.1% penicillin-streptomycin. HSkMC were differentiated in low glucose DMEM, 2% horse serum, 0.5 mg/mL BSA, 0.5 mg/mL fetuin, and 0.1% penicillin-streptomycin. C2C12 myoblasts were grown in high glucose DMEM (4.5 g/L glucose, [+]L-Glutamine; Gibco 11965-092) supplemented with 10% FBS (Heat Inactivated, Certified, US Origin; Gibco 10082-147), and 0.1% penicillin-streptomycin (10,000 U/mL; Gibco 15140122). C2C12 cells were differentiated into myotubes with low glucose DMEM (1 g/L glucose, [+]L-Glutamine, [+]110 mg/L sodium pyruvate; Gibco 11885-084) supplemented with 2% horse serum (Defined; VWR 16777), and 0.1% penicillin-streptomycin. For experiments with CI-976 C2C12 myoblasts were differentiated with either 10 μM of CI-976 or equal volume DMSO (vehicle). For experiments with methyl-beta-cyclodextrin cells were incubated with 10 mM (1320 g/mole) for 1 hour directly dissolved into media. For experiments with PDGF or EGF, C2C12 myotubes were incubated

with 2.5 ng/mL PDGF, 100 ng/mL EGF, or 12 nM insulin for 10 minutes. Prior to all experiments cells were serum-starved for 3 hours in low glucose DMEM containing 1% BSA and 0.1% penicillin-streptomycin.

Quantitative-RT-PCR

Samples were homogenized in TRIzol reagent (Life Technologies, Grand Island, NY) to extract total RNA. 1 µg RNA was reverse transcribed using IScript™ cDNA synthesis kit (Biorad, Hercules, CA). RT-PCR was performed with the Viia™ 7 Real-Time PCR System (Life Technologies, Grand Island, NY) using SYBR® Green reagent (Life Technologies, Grand Island, NY). All data were normalized to ribosomal L32 gene expression and primer sequences are provided (Extended Data Table 2).

Mass Spectrometry

Global lipidomic analyses for LN and OB HSkMC were performed at the Mass Spectrometry Resource at the Washington University School of Medicine (15). Extracted lipids with internal standards were analyzed with a Thermo Vantage triple-quadrupole mass spectrometer or a Thermo Trace GC Ultra mass spectrometer. Targeted lipidomic analyses for C2C12 myotubes and mouse skeletal muscles were conducted in the Metabolomics Core at the University of Utah (60-62). Extracted lipids with internal standards were analyzed with an Agilent triple-quadrupole mass spectrometer. The quantity of each lipid species was normalized to total lipid content for DRM/DSM experiments or to the total protein content for all others. The phospholipid saturation index was quantified by multiplying the relative abundance of each phospholipid species by the total number of double bonds in the acyl chains of that species.

Merocyanine 540

Merocyanine 540 (MC540) measurements were taken as previously described (63). In short, skeletal muscle cells (C2C12 and HSkMC) were fully differentiated and 2 million were used for measurements. Cells were washed with Hanks Balanced Salt Solution (HBSS; Gibco 14025092) prior to re-suspension in a cuvette with HBSS. MC540 in DMSO was added at a final concentration of 0.2 μM and after a 10-minute dark incubation, an emission scan was performed ranging from 550-750 nm with fluorescence excitation set at 540 nm on a PTI QuantaMaster 6000 Fluorimeter.

Lentivirus-Mediated Knockdown of LPCAT3

LPCAT3 expression was decreased using pLKO.1 lentiviral-RNAi system. Plasmids encoding shRNA for mouse LPCAT3 (shLPCAT3: TRCN0000121437) were obtained from Sigma (St. Louis, MO). Packaging vector psPAX2 (ID #12260), envelope vector pMD2.G (ID #12259) and scrambled shRNA plasmid (sc: ID1864) were obtained from Addgene (Cambridge, MA). HEK293T cells in 10 cm dishes were transfected using 50μL 0.1% Polyethylenimine, 200μL 0.15 M Sodium Chloride, and 500 μL Opti-MEM ([+] Hepes, [+] 2.4 g/L Sodium Bicarbonate, [+] L-Glutamine; Gibco 31985) with 2.66 μg of psPAX2, 0.75 μg of pMD2.G, and 3 μg of either scrambled or LPCAT3 shRNA plasmid. After 48 hours, growth media was collected, filtered using 0.22 μm vacuum filters, and used to treat undifferentiated HSkMC or C2C12 cells for 48 hours. To ensure only cells infected with shRNA vectors were viable, cells were selected with puromycin throughout differentiation.

Western Blot

Whole muscle or cells were homogenized and Western blots were performed as previously described (59). Protein homogenates were analyzed for abundance of phosphorylated(Tyr972)-insulin receptor (Invitrogen: 44-800G), insulin receptor-β (Cell Signaling: 3020S), phosphorylated(Thr308)-Akt (Cell Signaling: 9275S), phosphorylated(Ser472)-Akt (Cell

Signaling: 9271L), Akt (Cell Signaling: 9272S), phosphorylated(Thr642)-AS160 (Cell Signaling: 8881), AS160 (Millipore Sigma: 07-741), MyoD (DSHB: D7F2), mitochondrial complexes I-V (Abcam: ab110413), MHC type I (DSHB: A4.840), MHC type IIa (DSHB: SC-71), MHC type IIx (DSHB: 6H1), MHC type IIb (DSHB: BF-F3), MHC neo (DSHB: N1.551), MHC emb (DSHB: BF-G6), Caveolin-3 (BD Biosciences: 610-420), Na/K ATPase (Cell Signaling: 3010S), Flotillin-1 (Cell Signaling: 3253), and actin (Millipore Sigma: A2066).

Glycogen Synthesis

The glycogen synthesis rate was quantified as previously described (64, 65). Briefly, cells were incubated in media containing D-[U-^{14}C] glucose with (12 nM) or without insulin for 2h at 37 °C. Cells were then washed with ice-cold PBS and homogenized for 1h with 0.05% SDS. Part of the lysate was used for a protein assay and the other was combined with 2mg carrier glycogen and incubated at 100 °C for 1h. Ice cold ethanol (100%) was added to the boiled samples prior to overnight rocking at 4 °C. Samples were then centrifuged at 11,000 xG for 15 min at 4 °C to pellet glycogen. Pellets were re-suspended in de-ionized H_2O and glycogen synthesis was calculated with liquid scintillation.

Generation of LPCAT3 Skeletal Muscle-Specific Knock Out and Overexpressing Mice

Conditional LPCAT3 knock out (LPCAT3cKO+/+) mice were previously generated by flanking exon3 of the *Lpcat3* gene with *loxP* sites (25). LPCAT3cKO+/+ mice were then crossed with tamoxifen-inducible, skeletal muscle-specific Cre-recombinase (HSA-MerCreMer+/-) (34) mice to generate LPCAT3cKO+/+;HSA-MerCreMer-/- (Control; Ctrl) and LPCAT3cKO+/+;HSA-MerCreMer+/- (LPCAT3 Muscle-specific Knock-Out; LPCAT3-MKO). LPCAT3 conditional knock-in (LPCAT3cKI+/+) mice were generated by inserting a mouse LPCAT3 cDNA that was preceded by a lox-STOP-lox sequence into the Rosa26 locus of the genome. LPCAT3cKI+/+ mice were then crossed with HSA-MerCreMer+/- mice to generate control (LPCAT3cKI+/-;HSA-

MerCreMer-/-) and LPCAT3-MKI (LPCAT3 muscle-specific knocki-in, LPCAT3cKI+/-;HSA-MerCreMer+/-) mice. Tamoxifen injected (7.5 µg/g body mass, 5 consecutive days) control and LPCAT3-MKO/LPCAT3-MKI littermates were used for all experiments. Mice were maintained on a 12 h light/dark cycle in a temperature-controlled room. Prior to all terminal experiments and tissue harvesting, mice were given an intraperitoneal injection of 80 mg/kg ketamine and 10 mg/kg xylazine.

Glucose Tolerance Test

Intra-peritoneal glucose tolerance tests were performed by injecting 1 mg glucose/g body mass. Mice were fasted for 4 hours prior to glucose injection. Blood glucose was measured prior to glucose injection and 15, 30, 60, and 120 minutes post-injection via tail bleed with a handheld glucometer (Bayer Contour 7151H). In a separate set of experiments, mice were injected with 1 mg glucose/g body mass and blood was taken from the facial vein at the 30-minute time point for insulin quantification.

Serum Insulin and Glucose Quantification

Blood was collected from the facial vein either prior to anesthesia or at the 30-minute time point of the glucose tolerance test. Blood was then placed at room temperature for 20 minutes to allow for clotting before centrifugation at 2,000 xG for 10 minutes at 4°C. The supernatant (serum) was placed in a separate tube and stored at -80 °C until analysis.

Serum glucose was quantified using a colorimetric assay. A glucose standard curve was generated (Millipore Sigma, G6918) and serum samples were mixed with a PGO enzyme (Millipore Sigma, P7119) and colorimetric substrate (Millipore Sigma, F5803) and measured at OD450 on a plate reader. Serum insulin was quantified using an insulin mouse serum kit (CisBio, 62IN3PEF) using Fluorescence Resonance Energy Transfer on a plate reader (ThermoFisher, Varioskan LUX).

449

450 ***Hyperinsulinemic Euglycemic Clamp***

451 Hyperinsulinemic euglycemic clamps were performed as previously described (66-68). Briefly,
452 unrestrained mice were able to move freely while being continuously infused with insulin (2
453 mU/kg/min) and a variable infusion of 50% dextrose to allow for steady-state blood glucose of
454 approximately 150 mg/dL. Constant infusion of ^{3}H-glucose throughout the experiment and for 90
455 minutes prior to the clamp allowed for the quantification of glucose kinetics. At the end of a 2-
456 hour clamp ^{14}C-2-deoxyglucose (13 µCi/mouse) was administered during steady-state
457 conditions.

458

459 ***Ex Vivo Skeletal Muscle [^{3}H]2-Deoxy-D-Glucose Uptake***

460 *Ex vivo* glucose uptake was measured in the soleus muscle as previously described (69, 70). In
461 brief, soleus muscles were dissected and placed in a recovery buffer (KHB with 0.1% BSA, 8
462 mM glucose, and 2 mM mannitol) at 37 °C for 10 minutes. After incubation in recovery buffer,
463 muscles were moved to pre-incubation buffer (KHB with 0.1% BSA, 2 mM sodium pyruvate, and
464 6 mM mannitol) ± 200 µU/mL insulin for 15 minutes. After pre-incubation muscles were placed
465 in incubation buffer (KHB with 0.1% BSA, 9 mM [^{14}C]mannitol, 1 mM [^{3}H]2-deoxyglucose) ± 200
466 µU/mL insulin for 15 minutes. Contralateral muscles were used for basal or insulin-stimulated
467 measurements. After incubation muscles were blotted dry on ice-cold filter paper, snap-frozen,
468 and stored at -80 °C until analyzed with liquid scintillation counting.

469

470 ***Muscle Force Generation***

471 Force generating properties of extensor digitorum longus (EDL) muscles were measured as
472 previously described (71). Briefly, EDL muscles were sutured at each tendon and muscles were
473 suspended at optimal length (L_o) which was determined by pulse stimulation. After L_o was
474 identified muscles were stimulated (0.35 s, pulse width 0.2 ms) at frequencies ranging from 10-

200 Hz. Muscle length and mass were measured to quantify CSA (72-74) for force normalization.

Muscle Immunohistochemistry

Frozen, OCT-embedded hind limb muscle samples (tibialis anterior or EDL) were sectioned at 10μm using a cryostat (Microtome Plus™). Following 1h blocking with M.O.M mouse IgG blocking (Vector: MKB-2213), myofiber sections were incubated for 1h with concentrated BA.D5, SC.71, and BF.F3 (all 1:100; DSHB) and laminin (1:200; Millipore Sigma: L9393) in 2.5% normal horse serum. To visualize laminin (for fiber border), myosin heavy chain I (MHC I), myosin heavy chain IIa (MHC IIa), and myosin heavy chain IIb (MHC IIb), slides were incubated for 1h with the following secondaries: AMCA (1:250 Vector: CI-1000), Alexa Fluor 647 (1:250; Invitrogen: A21242), Alexa Fluor 488 (1:500; Invitrogen: A21121) and Alexa Fluor 555 (1:500; Invitrogen: A21426), respectively. Negatively stained fibers were considered myosin heavy chain IIx (MHC IIx). After staining, slides were coverslipped with mounting media (Vector: H-1000). Stained slides were imaged with a fully automated wide-field light microscope (Nikon, Nikon Corp.; Tokyo, Japan) with a 10X objective lens. Images were captured using high sensitivity Andor Clara CCD (Belfast, UK).

Administration of CI-976 In Vivo

CI-976 was administered as previously described (75). Briefly, C57BL/6J mice were fed a high-fat diet (Envigo: TD.88137) for 6 weeks before 7 consecutive days of subcutaneous injection of either vehicle (1:9 v:v of ethanol:polyethylene glycol [Rigaku Reagents: 1008414]) or CI-976 at a final concentration of 30 mg/kg.

GM-1 Labeling and Imaging

GM-1 clusters were labeled using a Vybrant® Alexa Fluor® 488 Lipid Raft Labeling Kit (ThermoFisher Scientific: V34404) as previously described (76). Briefly, 2 million myotubes were incubated 1mL in ice-cold starvation media with 0.8µg/mL fluorescent cholera toxin subunit B conjugate (CT-B) for 10 minutes. CT-B conjugates were then cross-linked with an anti-CT-B antibody (1:200) in ice-cold starvation media for 15 minutes. Cells were fixed for 1 h at 4 ˚C in ice-cold 4% paraformaldehyde in PBS in dark. Between each step, cells were washed 2x in ice-cold PBS. Cells were imaged on an Olympus FV1000 confocal microscope (2.5x, HV:600, offset: 30). Images were processed using NIH ImageJ. All images were background subtracted with a rolling ball radius of 50 pixels. Images were blindly scored by S.R.S and K.F. as exhibiting clustering of microdomains or non-clustering. Images were then subjected to color thresholding using the Otsu method (77, 78) (designed for thresholding images for cluster analyses) and made binary. A particle analysis of all particles that were >0.1µm^2 was performed to determine the average cluster size for each cell that was imaged (79). For each experiment, 35-50 cells per group were analyzed and the median was taken as a representative of that experiment.

Detergent-Resistant Membrane Isolation

Detergent-resistant membranes (DRM) and detergent-soluble membranes (DSM) were isolated as previously described (79). Briefly, 2x15 cm plates of cells were scraped in ice-cold PBS and then pelleted. Cells were re-suspended in 1mL of cold homogenization buffer (Mes-buffered saline [MBS], 1% Triton-X wt/v, and protease and phosphatase inhibitor) and passed through a 23-gauge needle 6 times before incubating at 4 °C for 30 minutes. MBS was added to the homogenate until a volume of 2.5 mL was reached then mixed with 2.5 mL of 90% sucrose in MBS and 4mL of this mixture was added to an ultracentrifuge tube (Beckman Coulter 344061). A sucrose gradient was generated by adding 4 mL 35% sucrose followed by 4mL of 5% sucrose. Samples were then centrifuged at 100,000 xG at 4 °C for 20 hours in a swinging bucket rotor (Beckman L8-M Ultracentrifuge, SW28 Rotor).

Statistics

Statistical analysis was performed using Prism 7 software (GraphPad). Student's t-tests were performed with data composed of 2 groups and 2-way ANOVA for multiple groups followed by Sidak's multiple comparison test. All data are Mean±SEM and statistical significance was set at $P<0.05$.

Study Approval

The experimental protocol was approved by the Internal Review Board for Human Research at East Carolina University. Informed consent was obtained prior to inclusion in the study.

Animal experiments were approved by the University of Utah Institutional Animal Care and Use Committee.

Author contributions

P.J.F. and K.F. contributed to study concept design and wrote the manuscript. J.A.H. performed human muscle biopsies. J.M.J. and M.J.D. contributed to study design and data analysis. X.R., P.T., T.D.G., J.M.M., and P.J.F. developed and maintained the mouse models. J.A.M., J.E.C., H.S., and J.T. performed mass spectrometry analyses. P.J.F., K.F., and S.R.S. performed analyses of the physical properties of phospholipid membranes. A.R.P.V. and P.J.F. performed analysis of muscle force production. P.S. performed muscle histology measurements. P.J.F. performed all biochemical assays and metabolic phenotyping measurements. K.C.K. and A.J.L. performed correlation analyses with 106 mouse strains. J.A.H., P.T., J.T., J.E.C., M.J.D., and S.R.S. edited the manuscript.

Acknowledgments

This work was supported by NIH grants DK107397, DK109888, AG063077 (to K.F.), DK108333, DK112826 (to W.L.H.), HL030568, HL030568, HL136618 (to P.T.), AT008375, ES031378 (to S.R.S.), HL028481, HL030568 (to A.J.L.), AG050781 (to M.J.D.), HL125695 (to J.M.M.), and DK056112 (to J.A.H.), American Heart Association 18PRE33960491 (to A.R.P.V.), American Heart Association 19PRE34380991 (to J.M.J.), and the Larry H. and Gail Miller Family Foundation (to P.J.F). The University of Utah Metabolomics, Mass Spectrometry, and Proteomics core is supported by S10 OD016232, S10 OD021505, and U54 DK110858. The Washington University Biomedical MS Resource is supported by United States Public Health Services grants P41-GM103422, P30-DK020579, and P30-DK056341.

References

1. Heron M. Deaths: Leading Causes for 2017. *National Vital Statistics Reports.* 2019;68(6).
2. Huo X, Gao L, Guo L, Xu W, Wang W, Zhi X, Li L, Ren Y, Qi X, Sun Z, et al. Risk of non-fatal cardiovascular diseases in early-onset versus late-onset type 2 diabetes in China: a cross-sectional study. *Lancet Diabetes Endocrinol.* 2016;4(2):115-24.
3. DeFronzo RA, Jacot E, Jequier E, Maeder E, Wahren J, and Felber JP. The effect of insulin on the disposal of intravenous glucose. Results from indirect calorimetry and hepatic and femoral venous catheterization. *Diabetes.* 1981;30(12):1000-7.
4. Thiebaud D, Jacot E, DeFronzo RA, Maeder E, Jequier E, and Felber JP. The effect of graded doses of insulin on total glucose uptake, glucose oxidation, and glucose storage in man. *Diabetes.* 1982;31(11):957-63.
5. DeFronzo RA, and Tripathy D. Skeletal muscle insulin resistance is the primary defect in type 2 diabetes. *Diabetes Care.* 2009;32 Suppl 2(S157-63.
6. Dube JJ, Coen PM, DiStefano G, Chacon AC, Helbling NL, Desimone ME, Stafanovic-Racic M, Hames KC, Despines AA, Toledo FG, et al. Effects of acute lipid overload on skeletal muscle insulin resistance, metabolic flexibility, and mitochondrial performance. *Am J Physiol Endocrinol Metab.* 2014;307(12):E1117-24.
7. Manco M, Mingrone G, Greco AV, Capristo E, Gniuli D, De Gaetano A, and Gasbarrini G. Insulin resistance directly correlates with increased saturated fatty acids in skeletal muscle triglycerides. *Metabolism.* 2000;49(2):220-4.
8. Lee JS, Pinnamaneni SK, Eo SJ, Cho IH, Pyo JH, Kim CK, Sinclair AJ, Febbraio MA, and Watt MJ. Saturated, but not n-6 polyunsaturated, fatty acids induce insulin resistance: role of intramuscular accumulation of lipid metabolites. *J Appl Physiol (1985).* 2006;100(5):1467-74.
9. Chavez JA, and Summers SA. Characterizing the effects of saturated fatty acids on insulin signaling and ceramide and diacylglycerol accumulation in 3T3-L1 adipocytes and C2C12 myotubes. *Arch Biochem Biophys.* 2003;419(2):101-9.
10. Bergman BC, Hunerdosse DM, Kerege A, Playdon MC, and Perreault L. Localisation and composition of skeletal muscle diacylglycerol predicts insulin resistance in humans. *Diabetologia.* 2012;55(4):1140-50.
11. Perreault L, Newsom SA, Strauss A, Kerege A, Kahn DE, Harrison KA, Snell-Bergeon JK, Nemkov T, D'Alessandro A, Jackman MR, et al. Intracellular localization of diacylglycerols and sphingolipids influences insulin sensitivity and mitochondrial function in human skeletal muscle. *JCI Insight.* 2018;3(3).
12. Adams JM, 2nd, Pratipanawatr T, Berria R, Wang E, DeFronzo RA, Sullards MC, and Mandarino LJ. Ceramide content is increased in skeletal muscle from obese insulin-resistant humans. *Diabetes.* 2004;53(1):25-31.
13. Schmitz-Peiffer C, Craig DL, and Biden TJ. Ceramide generation is sufficient to account for the inhibition of the insulin-stimulated PKB pathway in C2C12 skeletal muscle cells pretreated with palmitate. *J Biol Chem.* 1999;274(34):24202-10.
14. Itani SI, Ruderman NB, Schmieder F, and Boden G. Lipid-induced insulin resistance in human muscle is associated with changes in diacylglycerol, protein kinase C, and IkappaB-alpha. *Diabetes.* 2002;51(7):2005-11.
15. Paran CW, Verkerke AR, Heden TD, Park S, Zou K, Lawson HA, Song H, Turk J, Houmard JA, and Funai K. Reduced efficiency of sarcolipin-dependent respiration in myocytes from humans with severe obesity. *Obesity (Silver Spring).* 2015;23(7):1440-9.
16. Hulver MW, Berggren JR, Carper MJ, Miyazaki M, Ntambi JM, Hoffman EP, Thyfault JP, Stevens R, Dohm GL, Houmard JA, et al. Elevated stearoyl-CoA desaturase-1

expression in skeletal muscle contributes to abnormal fatty acid partitioning in obese humans. *Cell Metab.* 2005;2(4):251-61.
17. Lands WE. Metabolism of glycerolipides; a comparison of lecithin and triglyceride synthesis. *J Biol Chem.* 1958;231(2):883-8.
18. Fink KL, and Gross RW. Modulation of canine myocardial sarcolemmal membrane fluidity by amphiphilic compounds. *Circ Res.* 1984;55(5):585-94.
19. Bing RJ, Termin A, Conforto A, Dudek R, and Hoffmann MJ. Membrane function and vascular reactivity. *Biosci Rep.* 1993;13(2):61-7.
20. Hishikawa D, Hashidate T, Shimizu T, and Shindou H. Diversity and function of membrane glycerophospholipids generated by the remodeling pathway in mammalian cells. *J Lipid Res.* 2014;55(5):799-807.
21. Kazachkov M, Chen Q, Wang L, and Zou J. Substrate preferences of a lysophosphatidylcholine acyltransferase highlight its role in phospholipid remodeling. *Lipids.* 2008;43(10):895-902.
22. Zhao Y, Chen YQ, Bonacci TM, Bredt DS, Li S, Bensch WR, Moller DE, Kowala M, Konrad RJ, and Cao G. Identification and characterization of a major liver lysophosphatidylcholine acyltransferase. *J Biol Chem.* 2008;283(13):8258-65.
23. Pein H, Koeberle SC, Voelkel M, Schneider F, Rossi A, Thurmer M, Loeser K, Sautebin L, Morrison H, Werz O, et al. Vitamin A regulates Akt signaling through the phospholipid fatty acid composition. *FASEB J.* 2017;31(10):4566-77.
24. Koeberle A, Shindou H, Koeberle SC, Laufer SA, Shimizu T, and Werz O. Arachidonoyl-phosphatidylcholine oscillates during the cell cycle and counteracts proliferation by suppressing Akt membrane binding. *Proc Natl Acad Sci U S A.* 2013;110(7):2546-51.
25. Rong X, Wang B, Dunham MM, Hedde PN, Wong JS, Gratton E, Young SG, Ford DA, and Tontonoz P. Lpcat3-dependent production of arachidonoyl phospholipids is a key determinant of triglyceride secretion. *Elife.* 2015;4(
26. Parks BW, Sallam T, Mehrabian M, Psychogios N, Hui ST, Norheim F, Castellani LW, Rau CD, Pan C, Phun J, et al. Genetic architecture of insulin resistance in the mouse. *Cell Metab.* 2015;21(2):334-47.
27. Eto M, Shindou H, Koeberle A, Harayama T, Yanagida K, and Shimizu T. Lysophosphatidylcholine acyltransferase 3 is the key enzyme for incorporating arachidonic acid into glycerophospholipids during adipocyte differentiation. *Int J Mol Sci.* 2012;13(12):16267-80.
28. Martin SA, Gijon MA, Voelker DR, and Murphy RC. Measurement of lysophospholipid acyltransferase activities using substrate competition. *J Lipid Res.* 2014;55(4):782-91.
29. Li S, Song KS, and Lisanti MP. Expression and characterization of recombinant caveolin. Purification by polyhistidine tagging and cholesterol-dependent incorporation into defined lipid membranes. *J Biol Chem.* 1996;271(1):568-73.
30. Murata M, Peranen J, Schreiner R, Wieland F, Kurzchalia TV, and Simons K. VIP21/caveolin is a cholesterol-binding protein. *Proc Natl Acad Sci U S A.* 1995;92(22):10339-43.
31. Janes PW, Ley SC, and Magee AI. Aggregation of lipid rafts accompanies signaling via the T cell antigen receptor. *J Cell Biol.* 1999;147(2):447-61.
32. Chambers K, and Brown WJ. Characterization of a novel CI-976-sensitive lysophospholipid acyltransferase that is associated with the Golgi complex. *Biochem Biophys Res Commun.* 2004;313(3):681-6.
33. Chambers K, Judson B, and Brown WJ. A unique lysophospholipid acyltransferase (LPAT) antagonist, CI-976, affects secretory and endocytic membrane trafficking pathways. *J Cell Sci.* 2005;118(Pt 14):3061-71.
34. McCarthy JJ, Srikuea R, Kirby TJ, Peterson CA, and Esser KA. Inducible Cre transgenic mouse strain for skeletal muscle-specific gene targeting. *Skelet Muscle.* 2012;2(1):8.

35. Hishikawa D, Shindou H, Kobayashi S, Nakanishi H, Taguchi R, and Shimizu T. Discovery of a lysophospholipid acyltransferase family essential for membrane asymmetry and diversity. *Proc Natl Acad Sci U S A.* 2008;105(8):2830-5.
36. Gijon MA, Riekhof WR, Zarini S, Murphy RC, and Voelker DR. Lysophospholipid acyltransferases and arachidonate recycling in human neutrophils. *J Biol Chem.* 2008;283(44):30235-45.
37. Vainio S, Heino S, Mansson JE, Fredman P, Kuismanen E, Vaarala O, and Ikonen E. Dynamic association of human insulin receptor with lipid rafts in cells lacking caveolae. *EMBO Rep.* 2002;3(1):95-100.
38. Foti M, Porcheron G, Fournier M, Maeder C, and Carpentier JL. The neck of caveolae is a distinct plasma membrane subdomain that concentrates insulin receptors in 3T3-L1 adipocytes. *Proc Natl Acad Sci U S A.* 2007;104(4):1242-7.
39. Kabayama K, Sato T, Saito K, Loberto N, Prinetti A, Sonnino S, Kinjo M, Igarashi Y, and Inokuchi J. Dissociation of the insulin receptor and caveolin-1 complex by ganglioside GM3 in the state of insulin resistance. *Proc Natl Acad Sci U S A.* 2007;104(34):13678-83.
40. Hahn-Obercyger M, Graeve L, and Madar Z. A high-cholesterol diet increases the association between caveolae and insulin receptors in rat liver. *J Lipid Res.* 2009;50(1):98-107.
41. Capozza F, Combs TP, Cohen AW, Cho YR, Park SY, Schubert W, Williams TM, Brasaemle DL, Jelicks LA, Scherer PE, et al. Caveolin-3 knockout mice show increased adiposity and whole body insulin resistance, with ligand-induced insulin receptor instability in skeletal muscle. *Am J Physiol Cell Physiol.* 2005;288(6):C1317-31.
42. Oshikawa J, Otsu K, Toya Y, Tsunematsu T, Hankins R, Kawabe J, Minamisawa S, Umemura S, Hagiwara Y, and Ishikawa Y. Insulin resistance in skeletal muscles of caveolin-3-null mice. *Proc Natl Acad Sci U S A.* 2004;101(34):12670-5.
43. Deng YF, Huang YY, Lu WS, Huang YH, Xian J, Wei HQ, and Huang Q. The Caveolin-3 P104L mutation of LGMD-1C leads to disordered glucose metabolism in muscle cells. *Biochem Biophys Res Commun.* 2017;486(2):218-23.
44. Shang L, Chen T, Xian J, Deng Y, Huang Y, Zhao Q, Liang G, Liang Z, Lian F, Wei H, et al. The caveolin-3 P104L mutation in LGMD-1C patients inhibits non-insulin-stimulated glucose metabolism and growth but promotes myocyte proliferation. *Cell Biol Int.* 2019;43(6):669-77.
45. Huang Y, Deng Y, Shang L, Yang L, Huang J, Ma J, Liao X, Zhou H, Xian J, Liang G, et al. Effect of type 2 diabetes mellitus caveolin-3 K15N mutation on glycometabolism. *Exp Ther Med.* 2019;18(4):2531-9.
46. Shang L, Chen T, Deng Y, Huang Y, Huang Y, Xian J, Lu W, Yang L, and Huang Q. Caveolin-3 promotes glycometabolism, growth and proliferation in muscle cells. *PLoS One.* 2017;12(12):e0189004.
47. Simons K, and Toomre D. Lipid rafts and signal transduction. *Nat Rev Mol Cell Biol.* 2000;1(1):31-9.
48. Galbiati F, Engelman JA, Volonte D, Zhang XL, Minetti C, Li M, Hou H, Jr., Kneitz B, Edelmann W, and Lisanti MP. Caveolin-3 null mice show a loss of caveolae, changes in the microdomain distribution of the dystrophin-glycoprotein complex, and t-tubule abnormalities. *J Biol Chem.* 2001;276(24):21425-33.
49. Uhles S, Moede T, Leibiger B, Berggren PO, and Leibiger IB. Isoform-specific insulin receptor signaling involves different plasma membrane domains. *J Cell Biol.* 2003;163(6):1327-37.
50. Ogawa A, Firth AL, Smith KA, Maliakal MV, and Yuan JX. PDGF enhances store-operated Ca2+ entry by upregulating STIM1/Orai1 via activation of Akt/mTOR in human

pulmonary arterial smooth muscle cells. *Am J Physiol Cell Physiol.* 2012;302(2):C405-11.
51. Ohashi K, Nagata Y, Wada E, Zammit PS, Shiozuka M, and Matsuda R. Zinc promotes proliferation and activation of myogenic cells via the PI3K/Akt and ERK signaling cascade. *Exp Cell Res.* 2015;333(2):228-37.
52. Shulman GI. Cellular mechanisms of insulin resistance. *The Journal of clinical investigation.* 2000;106(2):171-6.
53. Chavez JA, and Summers SA. A ceramide-centric view of insulin resistance. *Cell metabolism.* 2012;15(5):585-94.
54. Kien CL, Bunn JY, Poynter ME, Stevens R, Bain J, Ikayeva O, Fukagawa NK, Champagne CM, Crain KI, Koves TR, et al. A lipidomics analysis of the relationship between dietary fatty acid composition and insulin sensitivity in young adults. *Diabetes.* 2013;62(4):1054-63.
55. Timmers S, Nabben M, Bosma M, van Bree B, Lenaers E, van Beurden D, Schaart G, Westerterp-Plantenga MS, Langhans W, Hesselink MK, et al. Augmenting muscle diacylglycerol and triacylglycerol content by blocking fatty acid oxidation does not impede insulin sensitivity. *Proc Natl Acad Sci U S A.* 2012;109(29):11711-6.
56. Demeure O, Lecerf F, Duby C, Desert C, Ducheix S, Guillou H, and Lagarrigue S. Regulation of LPCAT3 by LXR. *Gene.* 2011;470(1-2):7-11.
57. Yamazaki T, Hirose A, Sakamoto T, Okazaki M, Mitsumoto A, Kudo N, and Kawashima Y. Peroxisome proliferators attenuate free arachidonic acid pool in the kidney through inducing lysophospholipid acyltransferases. *J Pharmacol Sci.* 2009;111(2):201-10.
58. Lyu K, Zhang Y, Zhang D, Kahn M, Ter Horst KW, Rodrigues MRS, Gaspar RC, Hirabara SM, Luukkonen PK, Lee S, et al. A Membrane-Bound Diacylglycerol Species Induces PKC-Mediated Hepatic Insulin Resistance. *Cell Metab.* 2020;32(4):654-64 e5.
59. Heden TD, Ryan TE, Ferrara PJ, Hickner RC, Brophy PM, Neufer PD, McClung JM, and Funai K. Greater Oxidative Capacity in Primary Myotubes from Endurance-trained Women. *Med Sci Sports Exerc.* 2017;49(11):2151-7.
60. Heden TD, Johnson JM, Ferrara PJ, Eshima H, Verkerke ARP, Wentzler EJ, Siripoksup P, Narowski TM, Coleman CB, Lin CT, et al. Mitochondrial PE potentiates respiratory enzymes to amplify skeletal muscle aerobic capacity. *Science advances.* 2019;5(9):eaax8352.
61. Verkerke ARP, Ferrara PJ, Lin C-T, Johnson JM, Ryan TE, Maschek JA, Eshima H, Paran CW, Laing BT, Siripoksup P, et al. Phospholipid methylation regulates muscle metabolic rate through Ca2+ transport efficiency. *Nature Metabolism.* 2019;1(9):876-85.
62. Johnson JM, Verkerke ARP, Maschek JA, Ferrara PJ, Lin C-T, Kew KA, Neufer PD, Lodhi IJ, Cox JE, and Funai K. Alternative splicing of UCP1 by non-cell-autonomous action of PEMT. *Molecular Metabolism.* 2020;31(55-66.
63. Zeczycki TN, Whelan J, Hayden WT, Brown DA, and Shaikh SR. Increasing levels of cardiolipin differentially influence packing of phospholipids found in the mitochondrial inner membrane. *Biochem Biophys Res Commun.* 2014;450(1):366-71.
64. Park S, Turner KD, Zheng D, Brault JJ, Zou K, Chaves AB, Nielsen TS, Tanner CJ, Treebak JT, and Houmard JA. Electrical pulse stimulation induces differential responses in insulin action in myotubes from severely obese individuals. *J Physiol.* 2019;597(2):449-66.
65. Al-Khalili L, Chibalin AV, Kannisto K, Zhang BB, Permert J, Holman GD, Ehrenborg E, Ding VD, Zierath JR, and Krook A. Insulin action in cultured human skeletal muscle cells during differentiation: assessment of cell surface GLUT4 and GLUT1 content. *Cell Mol Life Sci.* 2003;60(5):991-8.

66. Holland WL, Miller RA, Wang ZV, Sun K, Barth BM, Bui HH, Davis KE, Bikman BT, Halberg N, Rutkowski JM, et al. Receptor-mediated activation of ceramidase activity initiates the pleiotropic actions of adiponectin. *Nat Med.* 2011;17(1):55-63.
67. Kusminski CM, Holland WL, Sun K, Park J, Spurgin SB, Lin Y, Askew GR, Simcox JA, McClain DA, Li C, et al. MitoNEET-driven alterations in adipocyte mitochondrial activity reveal a crucial adaptive process that preserves insulin sensitivity in obesity. *Nat Med.* 2012;18(10):1539-49.
68. Sharma AX, Quittner-Strom EB, Lee Y, Johnson JA, Martin SA, Yu X, Li J, Lu J, Cai Z, Chen S, et al. Glucagon Receptor Antagonism Improves Glucose Metabolism and Cardiac Function by Promoting AMP-Mediated Protein Kinase in Diabetic Mice. *Cell Rep.* 2018;22(7):1760-73.
69. Funai K, Lodhi IJ, Spears LD, Yin L, Song H, Klein S, and Semenkovich CF. Skeletal Muscle Phospholipid Metabolism Regulates Insulin Sensitivity and Contractile Function. *Diabetes.* 2016;65(2):358-70.
70. Funai K, Song H, Yin L, Lodhi IJ, Wei X, Yoshino J, Coleman T, and Semenkovich CF. Muscle lipogenesis balances insulin sensitivity and strength through calcium signaling. *The Journal of clinical investigation.* 2013;123(3):1229-40.
71. Ferrara PJ, Verkerke ARP, Brault JJ, and Funai K. Hypothermia Decreases O2 Cost for Ex Vivo Contraction in Mouse Skeletal Muscle. *Med Sci Sports Exerc.* 2018;50(10):2015-23.
72. Mendez JaK, A. . Density and Composition of Mammalian Muscle. *Metabolism.* 1960;9(4.
73. Moorwood C, Liu M, Tian Z, and Barton ER. Isometric and eccentric force generation assessment of skeletal muscles isolated from murine models of muscular dystrophies. *J Vis Exp.* 201371):e50036.
74. Brooks SV, and Faulkner JA. Contractile properties of skeletal muscles from young, adult and aged mice. *J Physiol.* 1988;404(71-82.
75. Krause BR, Anderson M, Bisgaier CL, Bocan T, Bousley R, DeHart P, Essenburg A, Hamelehle K, Homan R, Kieft K, et al. In vivo evidence that the lipid-regulating activity of the ACAT inhibitor CI-976 in rats is due to inhibition of both intestinal and liver ACAT. *J Lipid Res.* 1993;34(2):279-94.
76. Rockett BD, Teague H, Harris M, Melton M, Williams J, Wassall SR, and Shaikh SR. Fish oil increases raft size and membrane order of B cells accompanied by differential effects on function. *J Lipid Res.* 2012;53(4):674-85.
77. Otsu N. Threshold Selection Method from Gray-Level Histograms. *Ieee T Syst Man Cyb.* 1979;9(1):62-6.
78. Sezgin M, and Sankur B. Survey over image thresholding techniques and quantitative performance evaluation. *J Electron Imaging.* 2004;13(1):146-68.
79. Shaikh SR, Rockett BD, Salameh M, and Carraway K. Docosahexaenoic acid modifies the clustering and size of lipid rafts and the lateral organization and surface expression of MHC class I of EL4 cells. *J Nutr.* 2009;139(9):1632-9.

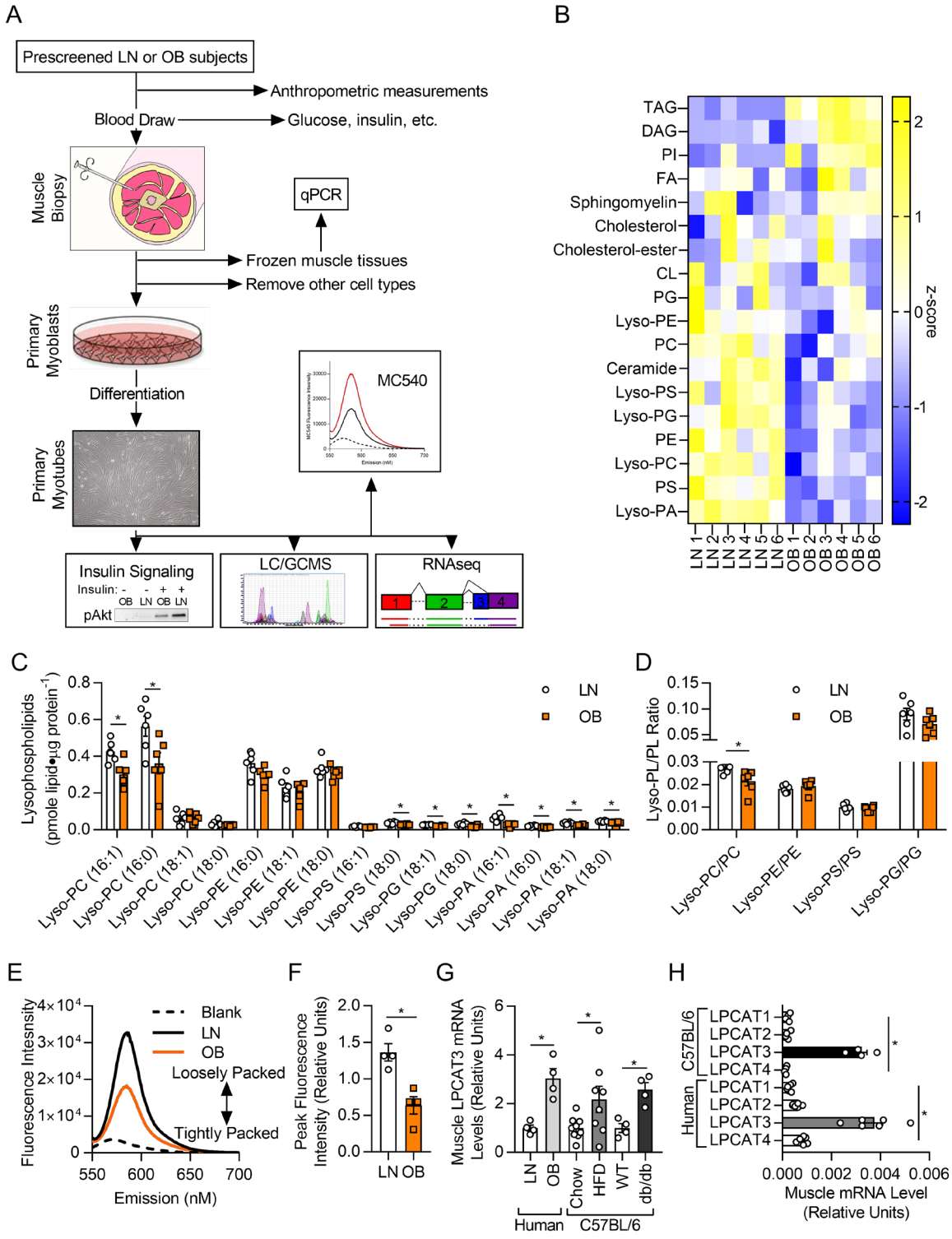

802

803 **Figure 1: Lipidomic analyses of skeletal muscle samples from human subjects that are**

804 **lean or with obesity.** (A) A schematic of the workflow for the clinical study. (B-D) Lipidomic

analysis of HSkMC from subjects that are insulin-sensitive and lean (LN) or insulin-resistant with obesity (OB). (B) Heat map of lipid content by class. (C) Species of lysophospholipids. (D) Lysophospholipid to phospholipid ratio (n=6). (E&F) Quantification of MC540 fluorescence in LN and OB HSkMC (n=4). (G) LPCAT3 mRNA in muscle biopsies from LN or OB subjects (left), in skeletal muscle of wildtype (WT) mice fed standard chow or high-fat diet (HFD) (middle), and in skeletal muscle of WT or db/db mice (right) (LN & OB: n=4, chow: n=9, HFD: n=8, WT & db/db: n=4). (H) Expression of all isoforms of LPCAT in muscle samples from mouse (n=4) or human (n=6) skeletal muscle. (C,D,F&G) Two-tailed t-tests. (H) One-way ANOVA followed by post-hoc multiple comparisons. All data are represented as mean ± SEM. *$P \leq 0.05$.

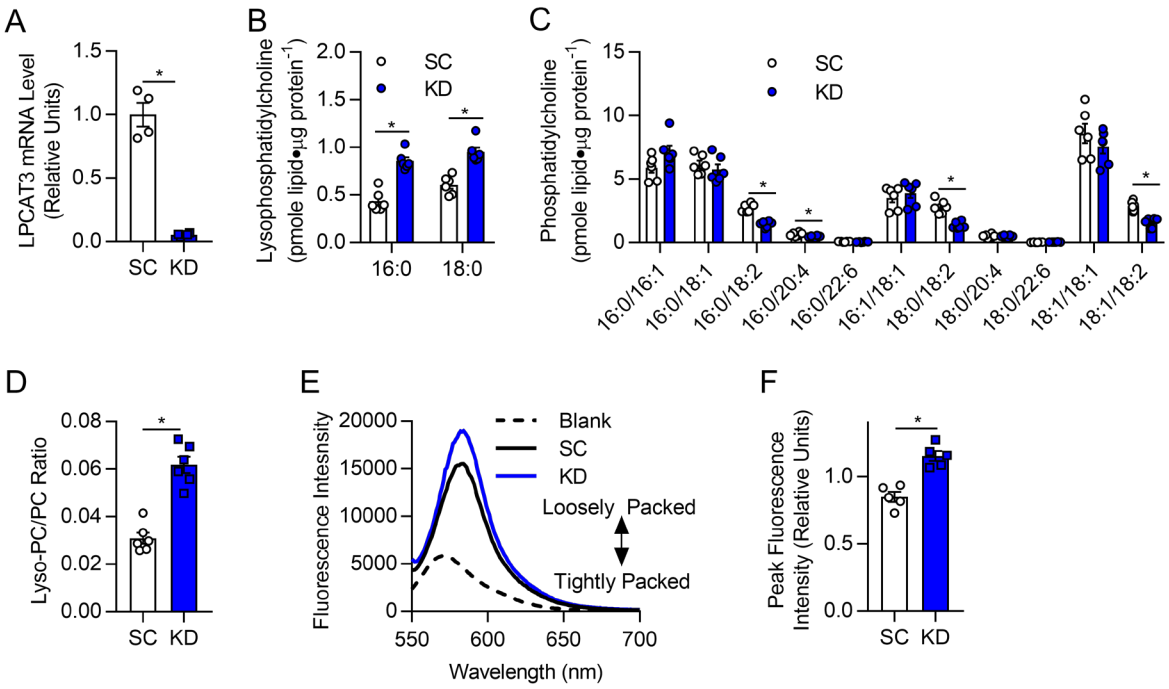

Figure 2: LPCAT3 knockdown alters skeletal muscle membrane phospholipid composition in vitro. (A) LPCAT3 mRNA levels in myoblasts infected with lentiviruses expressing shRNA for scrambled (SC) or LPCAT3 sequences (KD) and differentiated into myotubes (*n*=4). (B-D) Lipids were extracted from C2C12 myotubes for analysis between SC and KD cells. Quantification of (B) lysophosphatidylcholine (lyso-PC), (C) phosphatidylcholine (PC), and (D) total lyso-PC/PC (*n*=6). (E&F) Quantification of MC540 fluorescence in SC and KD myotubes (*n*=5). Two-tailed t-tests were performed. All data are represented as mean ± SEM. *$P \leq 0.05$.

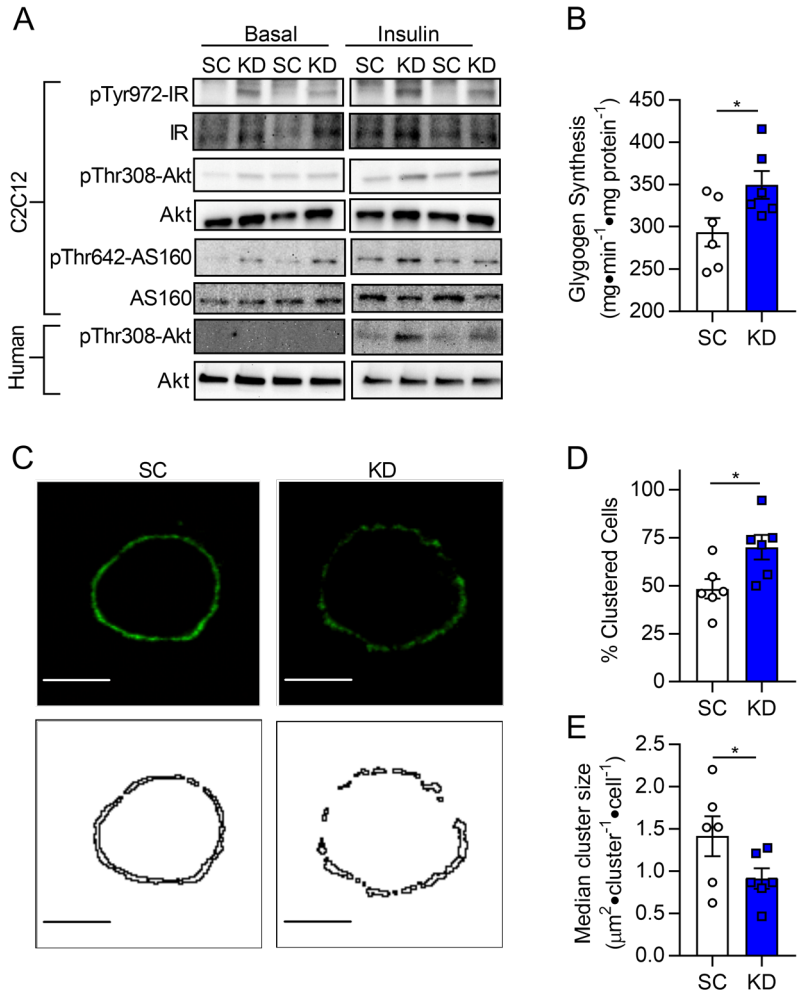

825

826 **Figure 3: LPCAT3 inhibition enhances skeletal muscle insulin sensitivity in vitro.**

827 Myoblasts were infected with lentivirus encoding scrambled (SC) or LPCAT3 knockdown (KD)

828 sequences and differentiated into myotubes. (A) Phosphorylation and total protein of IR, Akt,

829 and AS160 were measured via Western blot with (0.6 nM) or without insulin in C2C12 myotubes

830 (top) and human primary skeletal muscle cells (bottom) (image is representative from 3

831 experiments). (B) Glycogen synthesis was quantified in C2C12 cells incubated with insulin (12

832 nM) (*n*=6). (C-E) GM-1 enriched microdomains were labeled in SC and KD round-up myotubes.

833 (C) Plasma membrane GM-1 localization was visualized (top panels: fluorescence images,

834 bottom panels: binary images). (D) Cells were scored as clustered or non-clustered between SC

and KD myotubes. (E) Particle size was measured for each cell in 6 separate experiments and the median for each experiment was used as a representative of that experiment (n=35-50/experiment, 6 separate experiments). Two-tailed t-tests were performed. All data are represented as mean ± SEM. *$P \leq 0.05$.

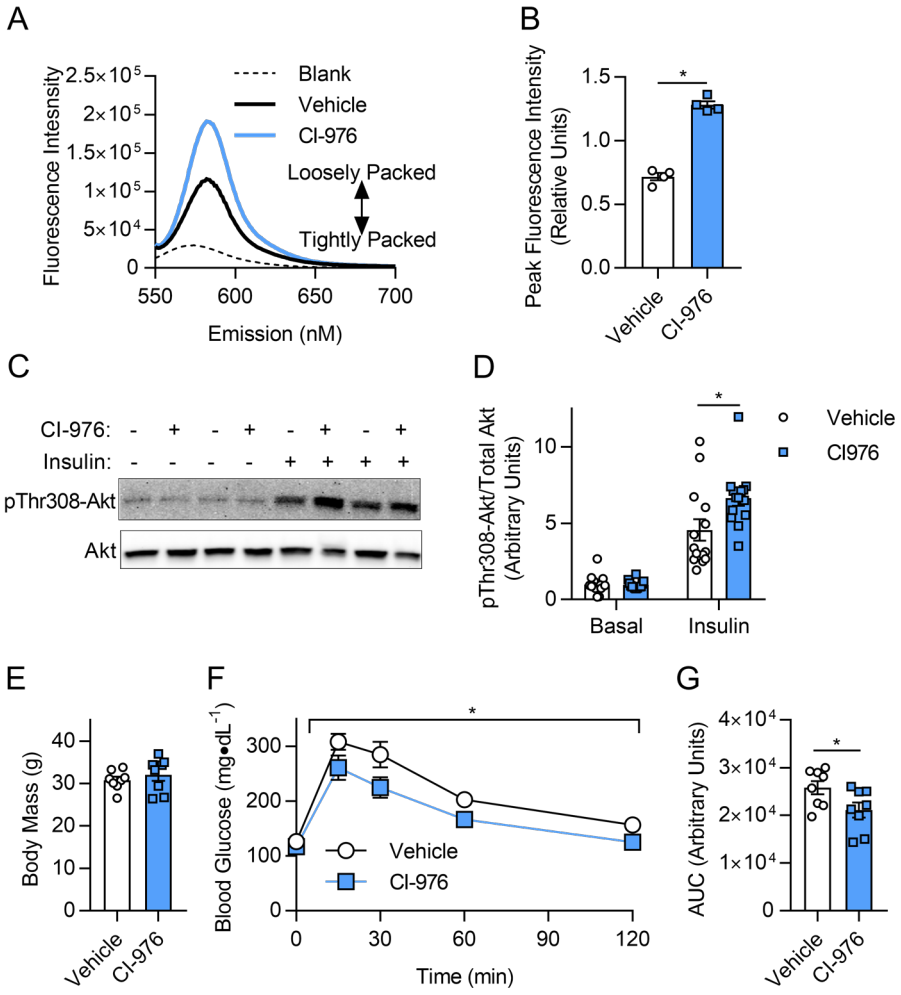

839

840 **Figure 4: Administration of CI-976 in vitro and in vivo.** (A-D) C2C12 myoblasts were
841 differentiated into myotubes with either CI-976 or vehicle. (A&B) Quantification of MC540
842 fluorescence (*n*=6). (C&D) Western blot and quantification of Thr308 phosphorylation and total
843 Akt in the presence (12 nM) and absence of insulin (*n*=14, P=0.024 main effect of insulin). (E-G)
844 Wildtype C57BL6/J mice were fed with HFD for 6 weeks with the last 7 days subcutaneously
845 injected with vehicle (1:9 ethanol:polyethylene glycol) or 30 mg•kg^{-1} CI-976. (E) Body mass, (F)
846 intraperitoneal glucose tolerance excursion curves, and (G) AUC from glucose tolerance tests
847 for vehicle-treated or CI-976 administered mice (*n*=8/group). (B,E&G) Two-tailed t-tests or

(D&F) 2-way ANOVA with Sidak's multiple comparisons test were performed. All data are represented as mean ± SEM. *$P \leq 0.05$.

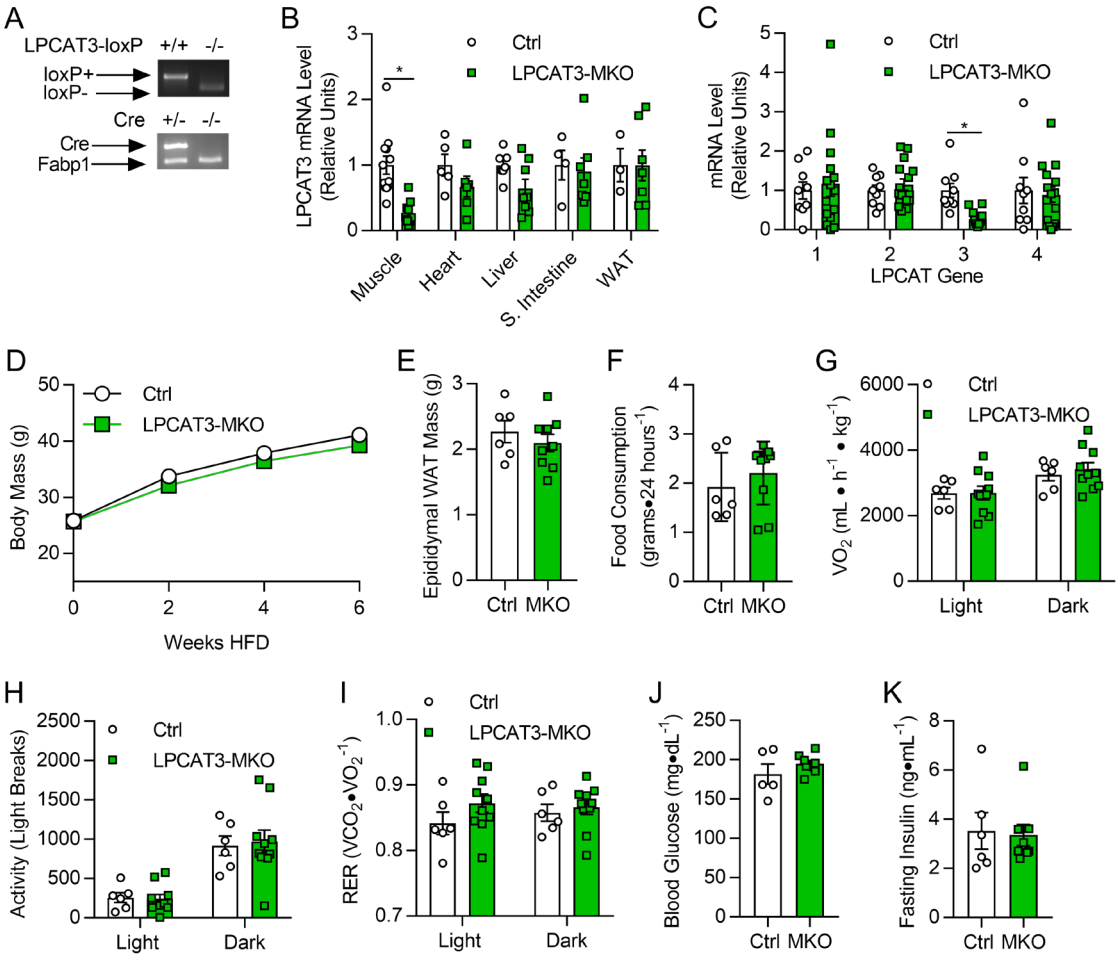

Figure 5: Whole-body phenotyping of LPCAT3-MKO mice. (A) Mice with tamoxifen-inducible skeletal muscle-specific Cre-recombinase (HSA-MerCreMer+/-) were crossed with mice with *LoxP* sites flanking exon3 of the *Lpcat3* gene (LPCAT3cKO+/+) to generate skeletal muscle-specific inducible knock out of LPCAT3 (LPCAT3cKO+/+, HSA-MerCreMer+/-) (LPCAT3-MKO). Littermates (LPCAT3cKO+/+, HSA-MerCreMer-/-) (Ctrl) were used as control mice for all experiments. (B) LPCAT3 mRNA in tibialis anterior (TA, Muscle), heart, liver, small intestine (S. Intestine), and inguinal white adipose tissue (WAT) (muscle: Ctrl *n*=12, MKO *n*=15; heart: Ctrl *n*=5, MKO *n*=6; liver: Ctrl *n*=7, MKO *n*=8; S. Intestine: Ctrl *n*=4, MKO *n*=7; WAT: Ctrl *n*=3, MKO *n*=7). (C) mRNA of all LPCAT isoforms in TA muscles of Ctrl and LPCAT3-MKO mice (Ctrl *n*=9, MKO *n*=14). (D) Body mass during high-fat diet (HFD) feeding in Ctrl and LPCAT3-MKO mice

(Ctrl *n*=8, MKO *n*=11). (E) Epididymal WAT mass (Ctrl *n*=6, MKO *n*=9). (F-I) Ctrl and LPCAT3-MKO mice were placed in metabolic chambers for measurement of (F) food consumption, (G) VO_2, (H) activity, and (I) respiratory exchange ratio (RER) (Ctrl *n*=6, MKO *n*=10). (J) Fasting glucose (Ctrl *n*=5, MKO *n*=9). (K) Fasting insulin (Ctrl *n*=6, MKO *n*=9). All data except (A) are from HFD-fed mice. (B,C,E,F,J&K) Two-tailed t-tests or (D,G,H&I) 2-way ANOVA with Sidak's multiple comparisons test were performed. All data are represented as mean ± SEM. *$P \leq 0.05$.

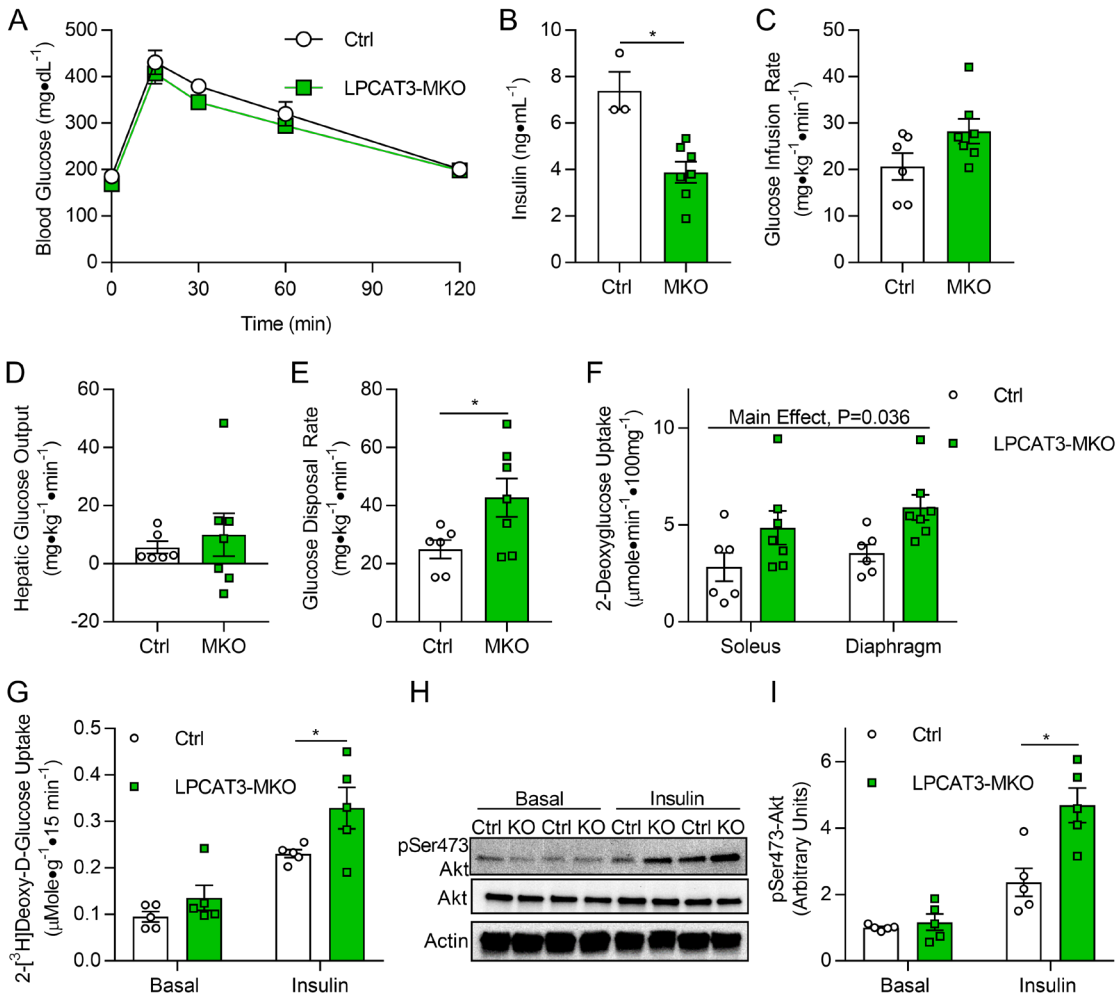

Figure 6: LPCAT3-MKO mice are protected from diet-induced skeletal muscle insulin resistance. (A) Intraperitoneal glucose tolerance test (Ctrl *n*=6, MKO *n*=8). (B) Serum insulin at the 30-minute time point of the glucose tolerance test (Ctrl *n*=3, MKO *n*=8). (C-F) Hyperinsulinemic-euglycemic clamps were performed in conscious unrestrained mice (Ctrl *n*=6, MKO *n*=7). (C) Glucose infusion rate required to maintain constant blood glucose of 150 mg•dL^{-1} during clamp phase. (D) Hepatic glucose output during the clamp phase. (E) Rate of whole-body glucose disposal during the clamp phase. (F) ^{14}C-2-deoxyglucose uptake quantification in soleus and diaphragm muscles during the clamped state. (G-I) Soleus muscles were dissected and incubated with or without 200 µU/mL of insulin. (G) *Ex vivo* 2-deoxyglucose uptake (*n*=5).

879 (H&I) Ser473 phosphorylation and total Akt (*n*=5). All data are from HFD-fed mice. (A,F,G&I) 2-
880 way ANOVA with Sidak's multiple comparisons test or (B,C,D&E) two-tailed t-tests were
881 performed. All data are represented as mean ± SEM. *$P \leq 0.05$.

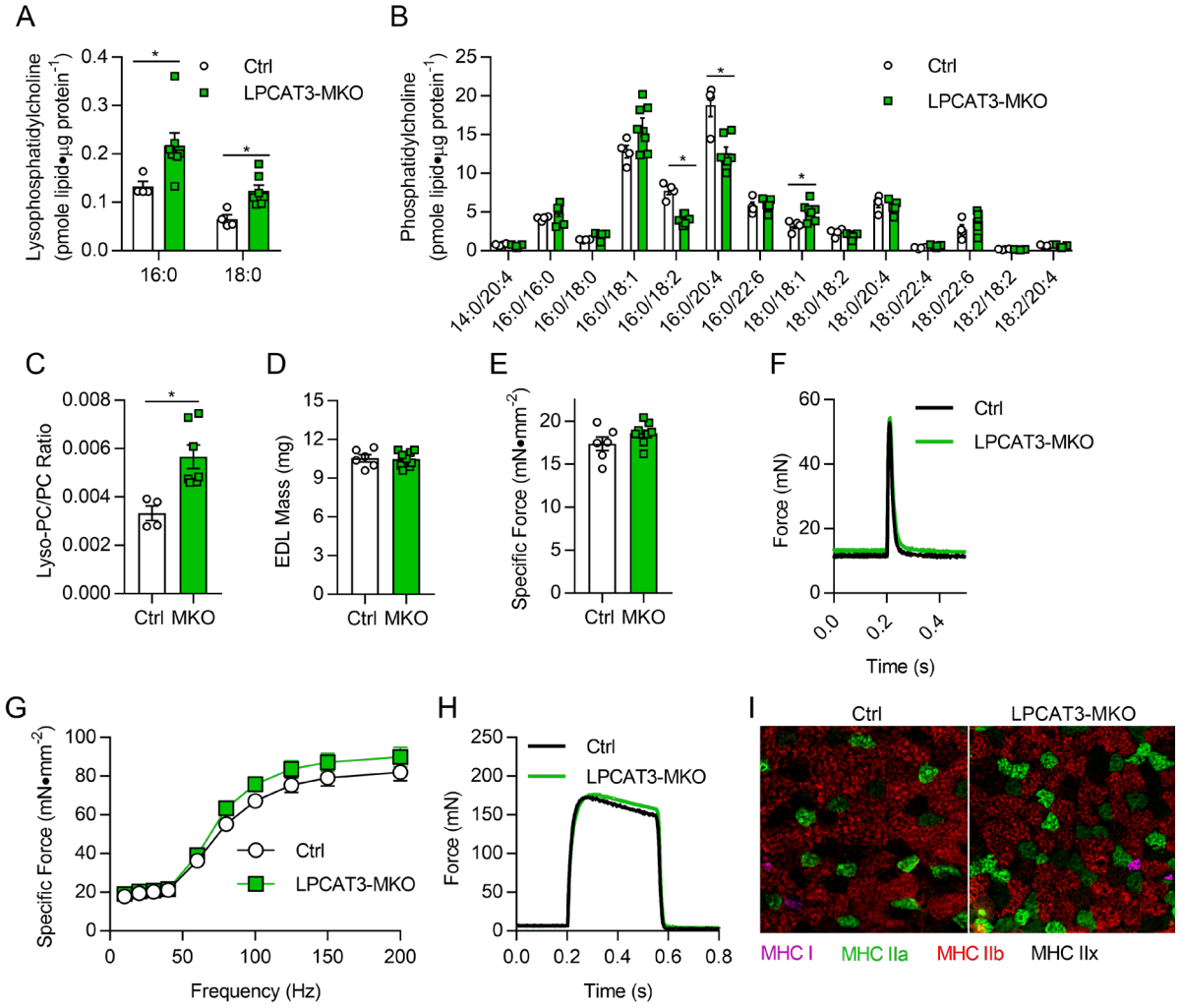

882

883 **Figure 7: Skeletal muscle lipid composition and contractility in LPCAT3-MKO mice.** (A-C)
884 Lipids were extracted from gastrocnemius muscles of Ctrl and LPCAT3-MKO mice for mass
885 spectrometric analysis. Quantification of (A) lyso-PC, (B) PC, and (C) total lyso-PC/PC (Ctrl *n*=4,
886 MKO *n*=7). (D-I) Extensor digitorum longus (EDL) muscles of Ctrl and LPCAT3-MKO mice were
887 dissected for measurement of (D) mass, (E&F) force produced with a pulse stimulation, (G&H)
888 force produced with tetanic stimulation ranging from 10-200 Hz (H, force tracing at 200 Hz
889 stimulation) (Ctrl *n*=6, MKO *n*=9), and (I) skeletal muscle fiber-type (MHC I: pink, MHC IIa:
890 green, MHC IIb:red, and MHC IIx: negative). (A-E) Two-tailed t-tests or (G) 2-way ANOVA with

891 Sidak's multiple comparisons test was performed. All data are represented as mean ± SEM. *P

892 ≤ 0.05.

893

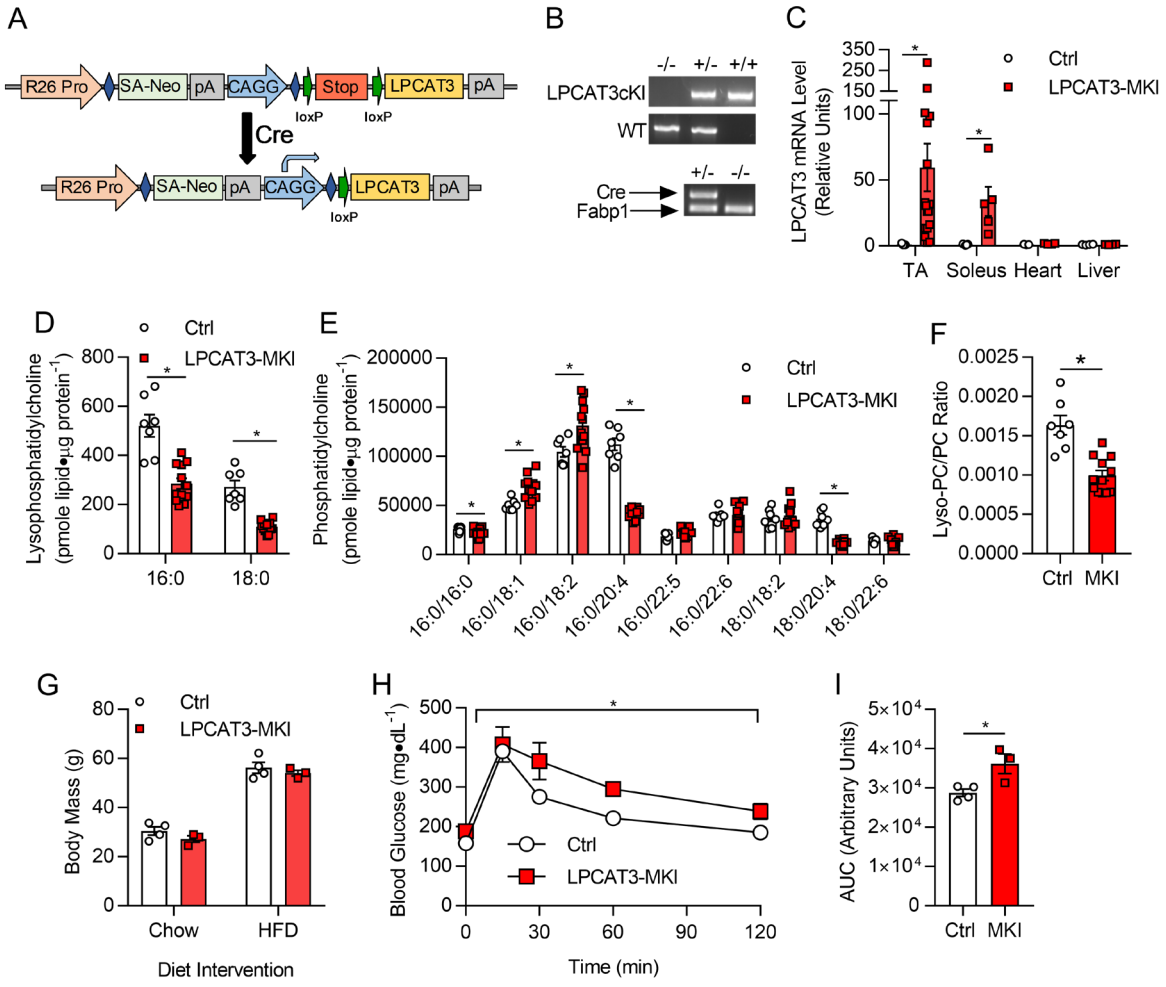

Figure 8: Generation and characterization of mice with skeletal muscle-specific overexpression of LPCAT3 (LPCAT3-MKI). (A) Schematic of LPCAT3 conditional knock-in (LPCAT3cKI+/+) mice with the insertion of mouse LPCAT3 cDNA sequence in the Rosa26 locus preceded by a Stop codon flanked with loxP sites. (B) Genotyping of LPCAT3cKI+/+ mice crossed with HSA-MCM+/- mice to generate LPCAT3cKI+/-; HSA-MCM-/- (Ctrl) or LPCAT3cKI+/-; HSA-MCM+/- (LPCAT3-MKI) mice. (C) Quantitative-RT-PCR of LPCAT3 in tibialis anterior (TA) (Ctrl *n*=9, MKI *n*=17), soleus (Ctrl *n*=5, MKI *n*=5), heart (Ctrl *n*=3, MKI *n*=4), and liver (Ctrl *n*=4, MKI *n*=4). (D-J) Lipids were extracted from TA muscles and quantified for (D) lysophosphatidylcholine (lyso-PC), (E) phosphatidylcholine (PC), (F) lyso-PC/PC ratio (Ctrl *n*=7,

MKI *n*=12). (G) Body mass of control and LPCAT3-MKI mice fed a standard chow diet or after 12 weeks of HFD feeding. (H) Intraperitoneal glucose tolerance test and (I) AUC from glucose tolerance test between control and LPCAT3-MKI mice after HFD feeding (Ctrl *n*=4, MKI *n*=3). (C-G&I) Two-tailed t-tests or (H) 2-way ANOVA was performed. All data are represented as mean ± SEM. *$P \leq 0.05$.

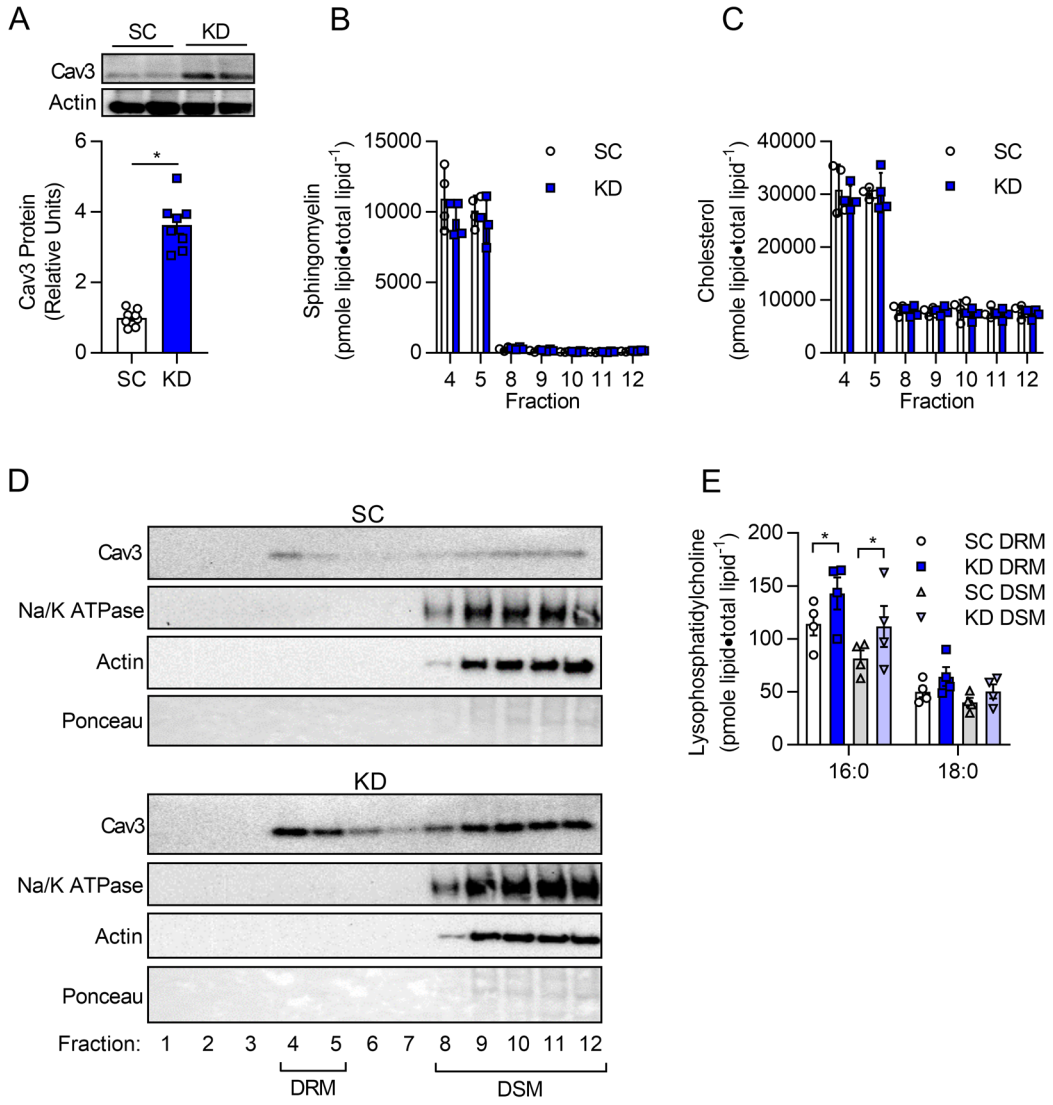

Figure 9: LPCAT3 deletion alters plasma membrane organization. C2C12 cells were infected with lentiviruses expressing shRNA for scrambled (SC) or LPCAT3 (KD) and differentiated into myotubes. (A) Caveolin-3 (cav3) protein content. (B&C) Detergent-resistant membranes (DRM; fractions 4&5) and detergent-soluble membranes (DSM; fractions 8-12) were isolated and lipids were extracted for quantification of (B) sphingomyelin and (C) cholesterol (*n*=4). (D) Cav3, Na/K ATPase, actin, and total protein content were assessed via Western blot in all fractions from the sucrose gradient (image is representative from 4 experiments). (E) Lyso-PC levels in DSM and DRM isolations (*n*=4). (A-C) Two-tailed t-tests or

(E) 2-way ANOVA with Sidak's multiple comparisons test were performed. All data are represented as mean ± SEM. *$P \leq 0.05$.

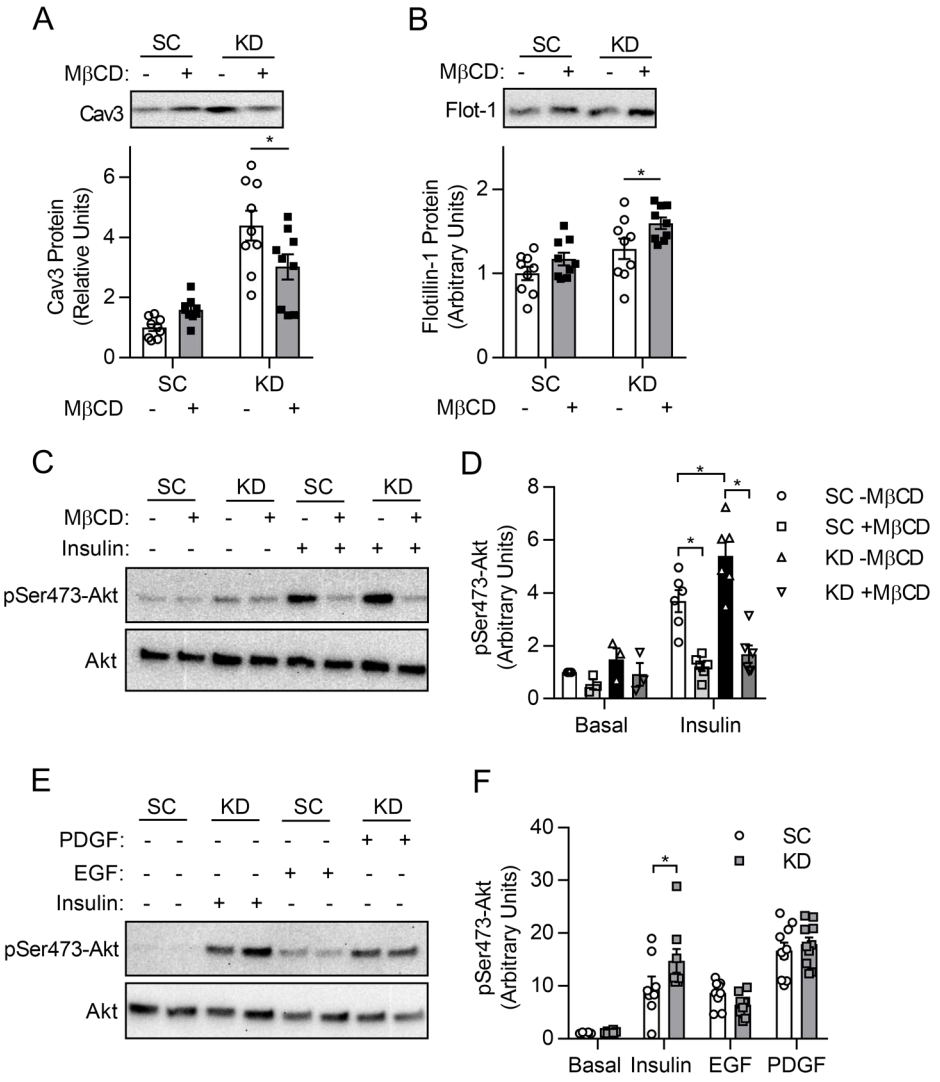

Figure 10: Disruption of caveolae is sufficient to normalize insulin signaling with LPCAT3 knockdown. C2C12 myoblasts were infected with lentivirus expressing shRNA for scrambled (SC) or LPCAT3 knockdown (KD) and were differentiated into myotubes. (A-D) Myotubes were incubated with or without 10 mM of methyl-β-cyclodextrin (MβCD) for 1hr. (A&B) MβCD successfully depletes cav3 ($P<0.001$, main effect of LPCAT3 knockdown) but not flotillin1 ($P=0.003$ main effect of LPCAT3 knockdown, $P=0.01$ main effect of MβCD) (n=9). (C&D) Cells were incubated in the presence (0.6 nM) or absence of insulin and were blotted for total or Ser473 phosphorylation of Akt (n=3 Basal, n=6 Insulin). (E&F) C2C12 myotubes were incubated

931 in the absence or presence of either PDGF (2.5 ng/mL), EGF (100 ng/mL), or insulin (12 nM)
932 and were blotted for total or Ser473 phosphorylation of Akt (Basal & Insulin, *n*=8, PDGF & EGF
933 *n*=10). 2-way ANOVA with Sidak's multiple comparisons test were performed. All data are
934 represented as mean ± SEM. **P* ≤ 0.05.
935

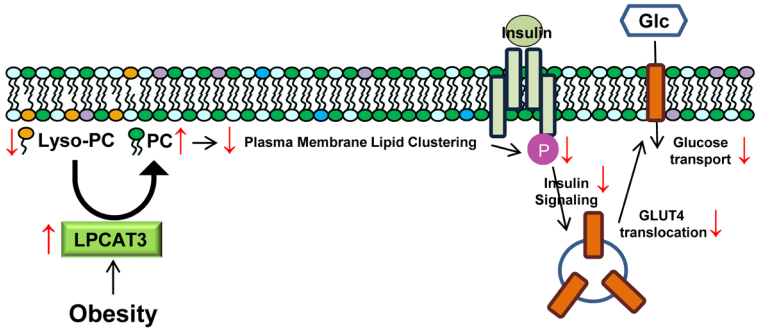

936

937 **Figure 11: A proposed mechanism of action by which LPCAT3 promotes diet-induced**

938 **skeletal muscle insulin resistance.**